UCRL- 91636, Rev. 1
PREPRINT

CIRCULATION COPY
SUBJECT TO RECALL
IN TWO WEEKS

Acetaldehyde Oxidation in the Negative Temperature Coefficient Regime: Experimental and Modeling Results

E. W. Kaiser
C. K. Westbrook
W. J. Pitz

This paper was prepared for submittal to
International Journal of Chemical Kinetics

July 11, 1985

Lawrence
Livermore
National
Laboratory

This is a preprint of a paper intended for publication in a journal or proceedings. Since changes may be made before publication, this preprint is made available with the understanding that it will not be cited or reproduced without the permission of the author.

DISCLAIMER

This document was prepared as an account of work sponsored by an agency of the United States Government. Neither the United States Government nor the University of California nor any of their employees, makes any warranty, express or implied, or assumes any legal liability or responsibility for the accuracy, completeness, or usefulness of any information, apparatus, product, or process disclosed, or represents that its use would not infringe privately owned rights. Reference herein to any specific commercial products, process, or service by trade name, trademark, manufacturer, or otherwise, does not necessarily constitute or imply its endorsement, recommendation, or favoring by the United States Government or the University of California. The views and opinions of authors expressed herein do not necessarily state or reflect those of the United States Government or the University of California, and shall not be used for advertising or product endorsement purposes.

Acetaldehyde Oxidation in the Negative Temperature Coefficient Regime: Experimental and Modeling Results

E. W. Kaiser
Ford Motor Company

C. K. Westbrook
W. J. Pitz
Lawrence Livermore National Laboratory

Abstract

Acetaldehyde oxidation at temperatures between 550 and 900 K has been studied in experiments carried out in a low pressure, static reactor and in numerical modeling calculations using a detailed chemical kinetic reaction mechanism. The results of the experimental study were used to construct and validate the reaction mechanism, which was then used to examine acetaldehyde oxidation in the negative temperature coefficient regime. This mechanism was also tested against independent measurements of acetaldehyde oxidation carried out by Baldwin, Matchan and Walker. The overall rate of reaction and the properties of the negative temperature coefficient regime were found to be sensitive to the competition between radical decomposition reactions and the addition of molecular oxygen to acetyl and methyl radicals. Implications of the results for future kinetic modeling of engine knock are discussed.

INTRODUCTION

The maximum compression ratio at which current spark-ignition engines can operate is limited because of the occurrence of knock. Since operation at higher compression ratio gives increased fuel efficiency, suppression of knock is a critical engine design goal [1]. One theory suggests that low temperature oxidation reactions in the end gas of the cylinder, which occur in the temperature range 500 K to 900 K, control the hot autoignition responsible for knock. This theory is based on the observation of cool flames and the existence of organic products characteristic of low temperature oxidation in the cylinder end gas prior to the occurrence of knock in engines [2-5]. To assess the importance of low temperature oxidation reactions in the initiation of knock, a better understanding of the chemical kinetic reaction mechanisms in this temperature range is needed. In addition, the well known negative temperature coefficient in the rate of consumption of organic fuels in this temperature regime leads to a variety of interesting oscillatory combustion phenomena whose chemical kinetic mechanisms are also not completely understood [6-8].

Aldehydes are reactive intermediate products formed during the low temperature oxidation of hydrocarbon fuels, and the determination of comprehensive reaction mechanisms [9] requires knowledge of aldehyde oxidation. Acetaldehyde is an observed intermediate in the oxidation of many fuel molecules and is particularly important in the combustion of ethanol, an alternate fuel and a cofuel in gasohol. Aldehydes also provide a source of alkyl radicals, and a study of acetaldehyde oxidation provides a method for testing and improving existing mechanisms of methyl radical oxidation in the low temperature regime.

This paper describes the results of a combined experimental and numerical modeling study of the oxidation of acetaldehyde in the temperature range 550-900 K. The experiments were carried out in a static reactor using techniques which have been applied previously to propionaldehyde oxidation [10]. A detailed chemical kinetic reaction mechanism has been developed to describe the experimental data, which includes the rate of acetaldehyde consumption and the yields of major intermediate and final product species. The results of our studies, which span the negative temperature coefficient region (553-713 K), complement those of other workers [11,12] who modeled acetaldehyde oxidation only in the higher temperature regime ($T \geq 1000$ K). In addition, a recent study [13] of acetaldehyde oxidation in a continuously stirred tank reactor (cstr) included kinetic modeling analysis which is consistent with the present work.

EXPERIMENTAL PROCEDURE

The oxidation experiments were carried out in a static, boric acid coated, one liter Pyrex reactor which was enclosed in a vacuum chamber and coupled to a mass spectrometer. The experimental apparatus, procedure, and boric acid passivation technique have been described in detail in a previous publication [10]. As a check of the surface passivation, the rate of reaction of a mixture of 60 torr H_2 + 150 torr O_2 was measured at 500 C at the beginning of each day of experiments. The maximum rate of H_2 consumption was measured to be 5.6 ($\pm$ 1.2) torr/minute with an induction period of $\approx$1.5 min, in satisfactory agreement with the values measured for a similar mixture by Baldwin and Major [13a] (7.1 $\pm$ 0.4 torr/min and 1.5 min, respectively). Kinetic measurements were performed at 553 K and 713 K using two initial oxygen concentrations (7×10^{16} and 8.3×10^{17} molecules/cm^3) and one CH_3CHO concentration (4.7×10^{16} molecules/cm^3). The total gas density was maintained at approximately 8.7×10^{17} molecules/cm^3 by adding either N_2 or argon to the fuel-oxygen mixture when using the lower O_2 concentration.

Each experiment was started by injecting premixed fuel, O_2, and diluent into the reactor. Beginning approximately 1-2 seconds after the injection, the CH_3CHO and major product concentrations were monitored as a function of time by molecular-beam mass spectrometry (MS). This allowed direct detection of CH_3O_2H (48 amu), H_2O_2 (34 amu), CH_3OH (31 amu), CH_2O (30 amu), CO (28 amu), and H_2O (18 amu). Each indicated mass number was essentially free of interference from other species under most experimental conditions.

During certain experiments, the entire contents of the reactor were removed after a selected reaction time for gas chromatographic (GC) analysis. This allowed measurement of the concentrations of CH_4, C_2H_6, CO_2, and CH_3CHO. It also provided a cross check of the concentrations of CH_3OH, CO, and CH_2O obtained from the mass spectrometer. The CO_2 and CH_3CHO parent masses both occur at 44 amu, and the rates of CH_3CHO consumption could not be determined directly from this mass. However, the GC analysis established and the modeling analysis confirmed that the CO_2 yield was constant throughout the course of the reaction. This measured yield was used to calculate and subtract the CO_2 interference from the 44 amu peak, providing a detailed concentration-time profile of CH_3CHO which agreed well with the isolated points determined by GC analysis. All product species concentrations were obtained by standardization of the MS or GC with the pure compound.

In repeat measurements of product yields and in cross comparisons of GC and MS data, the yields of most species were typically reproducible to ±15% of their mean values. The concentration of H_2O contained an additional absolute uncertainty of $\pm 2.5 \times 10^{15}$ molecules/cm^3 because of the large background noise in the MS at the parent mass. While the relative CH_3O_2H concentration was reproducible to ±10%, its absolute concentration is estimated to have a 25% uncertainty because of the difficulty of handling this relatively unstable compound in pure form for standardization of the mass spectrometer. The H_2O_2 concentration is also uncertain by approximately 25% for similar reasons. Product yields were measured at 553 K and 713 K using both argon and N_2 diluent gas during the low O_2 concentration runs; the yields were identical for both diluents.

EXPERIMENTAL RESULTS

During each experimental run at 553 K, the initial CH_3CHO concentration decreased exponentially with reaction time over a factor of 2.5, after the end of an induction period (see Figure 1). The effective first order decay rate constants determined from these experiments had standard deviations of ±5% from the mean values upon repeat measurements, and the plotted curves are compilations of several experiments. However, the induction periods varied substantially with temperature and initial O_2 density. At low initial O_2 concentration, the induction period at 553 K was 4-10 seconds, while for the high O_2 concentration the induction period at 553 K was reduced to 2-4 seconds. At 713 K, there was no observable induction period, and the CH_3CHO decay curve was still nearly exponential at low initial O_2 concentration (see Figure 2). Changing the inert diluent from argon to nitrogen produced no change in either the CH_3CHO consumption rates or the induction periods at either temperature. At the higher initial O_2 concentration, the decay rate was non-exponential at 713 K as shown in Fig. 2. Under these conditions, the initial decay rate was very rapid but then slowed after approximately 5 seconds. Because of the very rapid initial rate, product concentrations could be measured reliably only after approximately 50% of the initial acetaldehyde had been consumed, and the initial consumption rate of CH_3CHO was uncertain.

Figures 3-5 each show the mean product yield curves obtained from several repeat measurements of three initial conditions. Data in these figures are plotted as a function of the amount of CH_3CHO consumed for both initial O_2 concentrations at 553 K (Figs. 3 and 5) and for the low O_2 concentration at 713 K (Fig. 4). Table I presents the yields of products observed after consumption of 58% of the initial CH_3CHO for the high O_2 concentration experiments at 713 K. As discussed in the Experimental Procedure section, the measured product yields have uncertainties of approximately ±15% from the mean curves for all species with the exception of H_2O_2, H_2O and CH_3O_2H whose error limits are somewhat larger. In every case, the total amount of carbon contained in the products is 85-100% of that in the CH_3CHO consumed. Considering the error in the measured concentrations, this carbon balance is satisfactory. The yield of products is constant throughout the range of acetaldehyde conversions studied to within the ±15% measurement uncertainty for all molecules except CH_3O_2H and possibly CH_3OH. The yield of

CH_3O_2H increases later in the reaction by a significant amount. The yield of CH_3OH increases by a much smaller amount later in the reaction and may be nearly constant considering the 15% uncertainty.

In order to interpret these data, the principal reaction paths must be examined in detail. Competition between radical decomposition and reversible addition of molecular oxygen is a typical feature of low temperature oxidation. Important reactions of this type include

$$CH_3CO + M = CH_3 + CO + M \qquad (12)$$

$$CH_3CO + O_2 = CH_3CO_3 \qquad (13)$$

$$CH_3 + O_2 + M = CH_3O_2 + M \qquad (101)$$

At temperatures below 750 K, addition of O_2 to the methyl and acetyl radicals is very important not only in determining the product distributions but also in controlling the overall reaction rate, because the adduct species have a significant impact on the chain branching in the oxidation mechanism. In each case, one radical can produce one (propagation) or more (branching) product radicals. For methyl consumption, the main branching sequence of reactions is

$$CH_3 + O_2 = CH_3O_2 \qquad (101)$$

$$CH_3O_2 + CH_3CHO = CH_3O_2H + CH_3CO \qquad (10)$$

$$CH_3O_2H = CH_3O + OH \qquad (29)$$

For the acetyl radical, the sequence of reactions is

$$CH_3CO + O_2 = CH_3CO_3 \qquad (13)$$

$$CH_3CO_3 + CH_3CHO = CH_3CO_3H + CH_3CO \qquad (8)$$

$$CH_3CO_3H = CH_3CO_2 + OH \qquad (15)$$

$$CH_3CO_2 = CH_3 + CO_2 \qquad (21)$$

The decompositions of the methyl hydroperoxide and the peroxyacetic acid provide rapid growth of the radical pool. The experimental observation of significant amounts of CH_3O_2H in the products at 553 K confirms the presence of methylperoxy radicals and the existence of reactions 10 (or 22) in the reaction mechanism. CH_3O_2H is relatively stable, having a measured half life of approximately 80 sec at 553 K in our reactor (see Appendix). In contrast, peroxyacetic acid is too unstable to be present at sufficient quantity for measurement, having an estimated half life of approximately 1 sec [14].

Examination of reactions 12 and 13 suggests that changing the initial O_2 concentration should change the CO_2 yield relative to that of CO. Comparison of Figs. 3 and 5 shows that increasing the O_2 concentration does indeed increase the CO_2 and decrease the CO yield at 553 K, although the magnitude of the change is less than expected as will be discussed later. Increasing the temperature at constant initial O_2 and CH_3CHO density (compare Fig. 3 with 4 and Fig. 5 with Table I) drastically reduces the CO_2 yield. This results from the fact that the exothermic, reversible equilibrium of reaction 13, which strongly favors the acetylperoxy adduct at 553 K, is driven to the left at 713 K while the high activation energy decomposition reaction 12 occurs much more rapidly. Therefore, little CH_3CO_3 is present to lead to CO_2. The effect of O_2 concentration on the competition between reactions 12 and 13 is still visible at 713 K, however, and the CO_2 yield is substantially greater at high initial O_2 concentration. Note that this CO_2 formation mechanism differs from that at high temperatures where the only substantial path for production of CO_2 is the reaction

$$CO + OH = CO_2 + H \qquad (67)$$

Thus, there is a temperature regime near 550 K in the present case where a low temperature sequence of reactions produces CO_2 and a high temperature regime above about 900 K where reaction 67 produces CO_2. However, in the intermediate region of about 650-850 K, CO_2 production takes place only very slowly.

Comparison of the data at constant temperature but different O_2 concentration (Figs. 3 and 5 or Fig. 4 and Table I) shows that increasing the O_2 concentration raises the yield of CH_2O relative to that of CH_3OH, thereby increasing the ratio CH_2O/CH_3OH. This agrees with the expected competition between reactions 9 and 88

$$CH_3O + CH_3CHO = CH_3OH + CH_3CO \qquad (9)$$

$$CH_3O + O_2 = CH_2O + HO_2 \qquad (88)$$

in which methoxy radicals are converted into methanol and formaldehyde with relative yields which depend on the O_2 concentration.

Methane is formed by the abstraction of a hydrogen atom from CH_3CHO

$$CH_3CHO + CH_3 = CH_4 + CH_3CO \quad . \qquad (7)$$

Increasing the O_2 concentration decreases the observed CH_4 yield at both temperatures. This results from the shifting of the equilibrium in reaction 101 to the right, which decreases the methyl radical concentration. Conversely, increasing the temperature shifts this equilibrium to the left, forming more methyl radicals and increasing the methane yield. The observed changes in C_2H_6 concentration follow similar trends with changes in temperature and O_2 concentration since ethane is also formed from methyl radicals by the recombination reaction

$$CH_3 + CH_3 = C_2H_6 \qquad (-102)$$

The experimental results show the presence of significant amounts of H_2O under all conditions, and substantial H_2O_2 at 713 K when the higher initial O_2 concentration is used. Both products are expected to be formed in hydrogen abstraction reactions by OH and HO_2 radicals

$$OH + CH_3CHO = H_2O + CH_3CO \qquad (4)$$

$$HO_2 + CH_3CHO = H_2O_2 + CH_3CO \qquad (6)$$

and these observations confirm that OH and HO_2 are present during low temperature oxidation. Finally, no CH_3O_2H is observed at the higher temperature. This results from the fact that the homogeneous decomposition of CH_3O_2H via reaction 29 should become very fast by 713 K. At this temperature, we estimate a half life of approximately 0.02 sec based on our measured value at 553 K and an activation energy of 43 kcal/mol [14]. In addition, the production rate of CH_3O_2H is reduced at 713 K, since the equilibrium of reaction 101 is shifted substantially toward the $CH_3 + O_2$ side as temperature increases.

Thus, a low temperature oxidation mechanism containing the above reactions can explain the major qualitative features of the measured product yields. We now turn to a quantitative modeling of these experiments using a detailed reaction mechanism.

NUMERICAL MODEL AND REACTION MECHANISM

Acetaldehyde oxidation under the conditions described above has been simulated by assuming that the reaction takes place at constant volume and pressure. The heat of reaction was continuously removed from the system, maintaining a constant temperature. Since heat losses occur in the experiments only through the surface of the reaction vessel, spatial gradients in the temperature occur in a direction normal to the surface. However, if the pressure is low and the rate of heat release is small, these temperature gradients within the vessel are estimated to be very small ($\leq$10 K), and they have been neglected in the present modeling analysis. Only homogeneous gas phase reactions were considered, neglecting reactions which might occur at the surface of the reactor.

The chemical kinetics rate equations were integrated in time using the HCT program [15]. The detailed chemical kinetic reaction mechanism was assembled by combining a high temperature ($T \geq 900K$) mechanism for C_1-C_4 hydrocarbon oxidation [16] with other reactions which are generally believed to play a part in acetaldehyde oxidation for intermediate temperatures ($500\ K \leq T \leq 900\ K$). Some of these reactions have been presented in the previous section. Preliminary computations indicated that the C_3 and C_4 submechanisms could be deleted from the mechanism, since the predicted formation rates of C_3 and C_4 species from radical recombination reactions in these experiments were insignificant. The resulting mechanism was used to simulate the experimental data already discussed. Whenever possible, literature values were used for reaction rates. When no values were available, estimates were made by analogy to similar reactions. In some cases, rate constants were available only at room temperature, and activation energies have been estimated by using reasonable preexponential factors. The final reaction mechanism is given in Table II, showing both the forward and reverse rate parameters. Reverse reaction rates were computed from the forward rates and the appropriate equilibrium constants [17,18].

The application of this mechanism to the simulation of the experimental results indicated that many of the elementary reactions were insignificant over the present temperature range. Therefore, these steps could have been eliminated. However, the current mechanism is intended for future applications in which the temperatures can vary from 500 K to above 2000 K. As a result, mechanistic paths which may become important only at higher temperatures were retained.

COMPUTED RESULTS

A. Overall rate of reaction and product yields

Each of the four sets of initial conditions from the experimental study was simulated using the reaction mechanism in Table II, and a sensitivity analysis was carried out to determine which reactions had the greatest influence on the computed results. The computed rates of acetaldehyde consumption are compared with the experimental data in Figs. 1 and 2. Overall, the agreement is fairly good. The computed consumption rates for high initial O_2 concentration at both 553 K and 713 K agree well with the observed fuel consumption rates. For the diluted case (low initial O_2 concentration) at 713 K, the computed acetaldehyde consumption rate was also very close to the observations. However, the model results for low initial O_2 at 553 K indicate a rate of reaction which is approximately one half of that measured experimentally. No induction period is computed for either case at 713 K. At 553 K the calculated induction periods are about 3 seconds for the undiluted case and 14 seconds for the diluted case; these induction periods are consistent with the experimental data although the calculated value at low initial O_2 is somewhat longer than the experimental value, which may be affected by heterogeneous initiation reactions.

The computed product yields are compared with the experimental results in Figures 3-5 and in Table I. All of the observed trends are reproduced by the model, and the yields of all organic products agree with the experimental values to within ≈50% under all experimental conditions. The ratio of CO to CO_2 production increases dramatically with increasing temperature, due to the competition between Reactions 12 and 13 as discussed earlier. Computed yields of oxygenated species (CH_3OH, CH_2O, and CH_3O_2H) typically agree to within ± 50% with the experimental results for all initial conditions. This indicates that the predicted levels of CH_3O and CH_3O_2 are approximately correct and that the competition between reactions 9 and 88, which controls the relative yields of CH_2O and CH_3OH, is adequately treated in the mechanism. Predicted methane and ethane yields are very accurate at 713 K, where methane is a major product, and deviate by less than 30% from the experimental values at 553 K where the concentrations are much smaller. The experimental yield of methane changes by a factor of 250 and that of the ethane by more than 700 over the initial conditions studied; we believe that the predicted trends are in good agreement with experiment over this wide range of observed concentrations.

B. Reactions of CH_3, CH_3O, and CH_3O_2

The predicted methane and ethane levels depend strongly on the methyl radical concentration, being produced by the reactions

$$CH_3CHO + CH_3 = CH_3CO + CH_4 \qquad (7)$$

$$CH_3 + CH_3 = C_2H_6 \qquad (-102)$$

The CH_3 density and its variation as a function of temperature are very dependent on the equilibrium constant for reaction 101, the addition of O_2 to CH_3. Under the present conditions, this reaction is equilibrated at 713 K, so when the equilibrium is shifted to the right (by increasing the initial O_2), forming more CH_3O_2, the overall rate of chain branching increases markedly, leading to an increase in the rate of fuel consumption and decreases in the methane and ethane yields. The forward rate of reaction 101 was fixed originally at the experimentally determined third order rate [106]. Both the forward and reverse rate expressions were varied to produce the best overall agreement between the computed and experimental fuel consumption rates and product yields of methane and ethane. The computed sensitivity to this reaction was greater than any of the others in the mechanism. At 713 K the overall rate of fuel consumption as well as the product distributions depend strongly on the equilibrium constant for reaction 101; varying both forward and reverse reaction rate coefficients simultaneously by factors of two relative to the values in Table II produced computed results essentially identical to those summarized in Figs. 2 and 4 and Table I. At 553 K, the reaction is not equilibrated, but the single most sensitive reaction is the addition step for reaction 101.

Khachatryan et al. [103] and Slagle and Gutman [112] have measured K_{eq} for reaction 101 over the temperature range 694-811 K. The results of both experimental studies agree closely with each other. Preliminary results from the present modeling study provided satisfactory agreement with the experimental data only when a value for K_{eq} was used which was smaller than the experimental value at 713 K by a factor of four. In particular, predicted yields of CH_4 and C_2H_6 were much too low and predicted overall rates of acetaldehyde consumption were much too high if the experimental values for K_{eq} were used in the model. However, model analysis of the data of Slagle and Gutman [112] indicated that the preliminary mechanism was overpredicting the consumption of CH_3O_2 by the reaction

$$CH_3O_2 + CH_3 = CH_3O + CH_3O \quad . \qquad (23)$$

Similarly, in the acetaldehyde oxidation calculations, reaction 10

$$CH_3CHO + CH_3O_2 = CH_3CO + CH_3O_2H \qquad (10)$$

was also contributing substantially to the consumption of CH_3O_2. The rate of reaction 23 had been taken from the room temperature study of Parkes [32], assuming no temperature dependence of the reaction rate expression. However, it is possible that this reaction involves an addition step followed by the breaking of an O-O bond [113], for which a negative temperature dependence might be appropriate. In the final model mechanism indicated in Table II, the rate of reaction 23 is a factor of four smaller at the temperatures of this study than the room temperature value of Parkes. The original estimate of a rate expression for reaction 10 had been based on related measurements for reaction 84 with an activation energy of 9 kcal/mole. Computed results were found to agree better with experimental data if the rate of reaction 10 was reduced at both 553 K and 713 K to fit an expression

$$k_{10} = 3.57 \times 10^9 \exp(-5050/RT)\ \text{cm}^3/\text{mole-sec.}$$

As a result of reducing the rates of the alternative reactions consuming CH_3O_2 (i.e. reactions 10 and 23), values of k_{101} and K_{eq} for reaction 101 consistent with experimentally determined results could be used in the model calculations.

The temperature dependence of K_{eq} for reaction 101 in Table II is very slightly less than that determined by Khachatryan et al. [103] and by Slagle and Gutman [112] over their higher temperature range. However, in a recent measurement of the heat of formation of CH_3O_2 at 298 K, Kondo and Benson [111] estimate that $\Delta H_{298}(CH_3O_2) = 5.5 \pm 1$ kcal instead of the value 2.8 ±1.6 determined by Khachatryan et al. If this recent value is correct, the overall exothermicity of the addition reaction could be as much as 5 kcal smaller than that obtained by Khachatryan et al. This would more than account for the slightly smaller temperature dependence indicated from our data. Our determination is based on a fit to a complicated kinetic mechanism, and it is possible that the fit is not unique, particularly at the lower temperature where the concentrations of CH_4 and C_2H_6 are very small. The equilibrium constant expression used, however, does fit the measured yields of methane and ethane and the overall rate well over the temperature range 553 - 713 K.

The stable intermediate and product species H_2O, CH_3OH, CH_4, and H_2O_2 are all produced primarily by H atom abstraction from the acetaldehyde fuel by the reactions

$$CH_3CHO + OH = CH_3CO + H_2O \quad (4)$$

$$CH_3CHO + CH_3O = CH_3CO + CH_3OH \quad (9)$$

$$CH_3CHO + CH_3 = CH_3CO + CH_4 \quad (7)$$

$$CH_3CHO + HO_2 = CH_3CO + H_2O_2 \quad (6)$$

The rate of reaction 9 has been measured previously only at room temperature [26], where the rate of reaction 88 was used as a reference. More recent determinations [69,70] have modified the rate of reaction 88, so that reanalysis of the results of Kelly and Heicklen [26] would suggest a slight increase in the derived rate of reaction 9 at room temperature. By combining the rate required to fit our data at 553K and 713K with the revised room temperature value, the activation energy of this reaction can be estimated to be 1.28 kcal/mole. In addition, CH_3O_2H is formed by the two reactions

$$CH_3CHO + CH_3O_2 = CH_3CO + CH_3O_2H \quad (10)$$

$$CH_3O_2 + HO_2 = CH_3O_2H + O_2 \quad (22)$$

It is possible to adjust the rates of reactions 6, 9, 10, 22, and 88 by ≤ 50% to improve the fit to the species product yields for any one set of experimental data. However, predicted product yields are higher than experimentally observed results in some cases and are lower in other cases. For example, the computed ratio of methanol to formaldehyde is somewhat too high in the 713 K diluted case and slightly too low in the undiluted case at the same temperature. Similarly, the computed ratio of CO to CO_2 at 553 K is too high in the diluted case and too low in the undiluted case. The agreement between computed and experimental values for one or two particular species could be improved by varying several reaction rates, but these variations would cause the agreement for other species to deteriorate. We have already discussed how the ratio of methanol to formaldehyde depends on the competition between reactions 9 and 88 of the methoxy radical. In the undiluted case at 553 K, more than 80% of the methoxy radical consumption takes place by reaction 88 with O_2, while this path accounts for only 30% of the methoxy radical consumption in the diluted case. Variations in k_9 and k_{88} did improve the computed methanol and formaldehyde yields at 553 K, but these changes also accelerated the rate of fuel consumption for the undiluted case (Case B in Fig. 1) to an unacceptable degree while the rate of fuel consumption was unchanged in the diluted case (Case A in Fig. 1). The present kinetic mechanism therefore represents a weighted compromise over the experimental data used to test and evaluate the model.

C. Reactions determining the CO and CO_2 yields

In the low O_2 case at 553K, the model underpredicts the CO_2 yield by about a factor of two, while the predicted CO_2 yield is somewhat too high in the high initial O_2 case. During the computational sensitivity analysis, it was found that the production of CO_2 is controlled almost exclusively by the rate of reaction 13 relative to that of reaction 12. When the ratio k_{13}/k_{12} is increased, the ratio of CO_2 to CO increases. Therefore, any change in k_{13} to improve the agreement at 553 K in one case results in worse agreement in the other case. An increase in k_{13} relative to k_{12} also has the effect of accelerating the rate of fuel consumption because of the increased chain branching as discussed earlier. If the rate constants for reactions 12 and 13 are both changed by the same factor, the mechanism predicts no change in either the product yields or the overall rates of reaction. Thus, the mechanism in Table II is sensitive only to the relative values of k_{12} and k_{13} and not to their absolute values for changes of up to a factor of 100 in the rate constants.

The rates of both reactions 12 and 13 are uncertain in this pressure and temperature region. For the rate of reaction 12, we have chosen the high pressure value measured by Watkins and Word [107] multiplied by an estimated falloff parameter. The rate of reaction 13 was adjusted to give a reasonable fit to the CO_2/CO ratio for the high initial O_2 concentration experiments at 553 K. This fit to reaction 13, when combined with the room temperature measurement of this rate [28] yields a negative activation energy of 2.7 kcal/mole for the addition reaction. The magnitude of this negative activation energy is quite reasonable since negative activation energies of 2.0 and 2.2 kcal have been determined for addition of O_2 to ethyl [108] and n-propyl [109] radicals.

Another measurement of the rate constant for reaction 12 by O'Neal and Benson [110] is available. The high pressure limiting rate determined by extrapolation from these low pressure measurements is much smaller than that of Watkins and Word, and the preexponential factor is abnormally low for a unimolecular reaction. However, the second order limiting rate constant determined by O'Neal and Benson, which is a factor of 10 below the value used in Table II, was measured in the same temperature and pressure range used in our experiments. Thus, it is possible that the rate constant in Table II could be at least a factor of 10 too large. If a smaller value of the rate of reaction 12 were adopted, the rate constant for reaction 13 would have to be reduced by the same amount to maintain the same CO_2/CO

ratio and the same overall rate of acetaldehyde consumption. A reduction of this rate constant constant at 553 K would also be acceptable because it is likely that the reaction will have entered the second order falloff regime at this elevated temperature, even though at room temperature the rate appears to be pressure independent at 2-4 torr [28]. Support for this suggestion is provided by the observation that the addition of O_2 to ethyl radicals is entering the falloff region at a pressure of about 10 torr and a temperature of 298 K [28].

Within the constraints placed on the kinetic mechanism in Table II by all four sets of experiments, it was not possible to find a single set of rate parameters which would bring these CO and CO_2 values at 553 K into simultaneous agreement. This discrepancy may be the result of inadequacies in the reaction mechanism which are significant only at the lowest end of the temperature range being considered. A number of reactions involving CH_3CO_3 are included in the reaction mechanism which do not involve H atom abstraction from acetaldehyde (Reactions 14-20), but the computations did not demonstrate sufficient sensitivity to these reaction rates to be able to refine this part of the mechanism. It is possible that additional reaction paths, omitted from the present mechanism, may contribute to the overall rate of reaction and the rate of CO_2 production. In the high O_2 case, the addition reaction

$$CH_3CO + O_2 = CH_3CO_3 \qquad (13)$$

will be faster, and the omission of other low temperature reactions of the acetyl radical would not be as important, but at lower O_2 concentrations, such omissions might become more significant.

If reactions 12 and 13 are the major paths for forming CO and CO_2, the ratio CO_2/CO should be nearly proportional to the initial O_2 concentration as is predicted by the mechanism. Thus, the ratio is predicted to increase by approximately a factor of 9.4 when the initial O_2 concentration is increased by a factor of 11.8. The experimentally determined ratio, including the estimated ±15% error in the measured values, increases by only a factor of 1.8 ± 0.8. This suggests the existence of a CO_2 formation mechanism, either homogeneous or surface-catalyzed, whose rate is not directly dependent on initial O_2 concentration. Possible homogeneous reactions which could fit this requirement are

$$CH_3CO + CH_3O_2 = CH_3CO_2 + CH_3O \qquad (154)$$

$$CH_3CO + HO_2 = CH_3CO_2 + OH \qquad (155)$$

followed by reaction 21. These reactions have not been observed but are analogous to the reaction of methyl radicals with CH_3O_2 (23) and HO_2 (100), which have very fast rate constants. Because the calculated steady-state concentrations of CH_3O_2 and HO_2 only increase by a factor of two when the initial O_2 increases by a factor of 12, these paths would provide a source of CO_2 formation which has a less than first order dependence on O_2 concentration. If the rates of these acetyl + RO_2 reactions are assumed equal to their methyl radical counterparts and no other reaction rates are changed, the calculated CO_2 yield remains essentially unchanged. This happens because reaction 13 consumes acetyl radicals to form CO_2 ten times faster than the sum of reactions 154 and 155 even at low initial O_2 concentration. However, as has been discussed previously, the rate constants for the addition of O_2 to CH_3CO and the decomposition of CH_3CO may be considerably slower at 553 K than those presented in Table II. If these rates were slower by a factor of about 30, then the CO_2 generation by reactions 154 and 155 would be significant and would double the CO_2 yield at low initial O_2 concentration. Calculations using such a revised mechanism show better agreement with the observed oxygen dependence of the CO/CO_2 ratio at 553 K.

A less than linear dependence of the rate of CO_2 formation on O_2 concentration has also been observed by Baldwin et al. [19], while studying the oxidation of propionaldehyde at 713 K. At this temperature, the CO_2 yield is relatively small (≈ 4%). These authors suggest that this effect may result from a surface reaction forming CO_2 according to the overall rate expression:

$$\frac{d[CO_2]}{dt} = k_s\,[C_2H_5CHO]\,[O_2]^{0.5} \quad . \qquad (156)$$

We did not vary the surface-to-volume ratio in these experiments and cannot draw conclusions about the contribution of heterogeneous reactions to product formation. However, a heterogeneous reaction of this type would be expected to have a positive activation energy, and the absolute rate of heterogeneous formation of CO_2 should be slower at 553 K than at 713 K. The measured rate of consumption of acetaldehyde at 553 K and low initial O_2 concentration is similar to that at 713 K. Thus, the CO_2 yield at 553 K resulting from heterogeneous reaction should be of similar magnitude or smaller than that at 713 K. Since the total CO_1 yield at 553 K is a factor of 30 greater than that at 713 K, it seems unlikely that a heterogeneous reaction of the type discussed above would be responsible for the unexplained variation of the CO_2/CO ratio with changes in O_2

concentration. If reaction 156 were responsible, a value of k_s with an improbable negative 17.5 kcal/mole activation energy would be required. Note that the importance of either reactions 154, 155, or 156 decreases in comparison to reaction 13 at high initial O_2 concentration.

In order to verify the importance of a proposed homogeneous formation of CO_2 via reactions 154 and 155, experimental measurements of these rates and of the rates of reactions 12 and 13 in the higher temperature falloff regime are needed. If such reactions can be observed, these reactions should be considered in any mechanism for modelling oxidation of aldehydes in this temperature regime.

MODELING OF THE NEGATIVE TEMPERATURE COEFFICIENT REGIME

A. Predicted rate of acetaldehyde consumption

The experimental results indicate a nearly equal rate of fuel consumption at both 553 K and 713 K for the case in which the lower initial O_2 concentration is used. This observation is consistent with the existence of a region of negative temperature dependence in the overall rate of acetaldehyde oxidation, as reported previously by Baldwin et al. [20]. Once the computations provided reasonably accurate results at these two temperatures, the model was used to predict the rate of acetaldehyde oxidation over an extended range of temperature from about 550 K to nearly 900 K. Computations were carried out for both the diluted and undiluted cases, each at constant density, with the pressure varying with the temperature.

The maximum rates of fuel consumption for both the diluted and undiluted cases are plotted as Curves A and B, respectively, in Fig. 6. These curves indicate clearly the existence of a region of negative temperature coefficient between about 650 K and 750 K, more pronounced in the diluted case. It is now well established that this negative temperature coefficient is the result of a gradual shift with temperature in the equilibrium of addition reactions such as reactions 13 and 101. As the equilibria shift away from the adduct sides, the sharply reduced rates of chain branching already discussed above result in a net reduction in the overall rate of fuel consumption. This phenomenon is related to the concept of a "ceiling temperature" discussed originally by Benson [21].

Recently, Morgan et al. [104] re-evaluated Benson's values for the ceiling temperature (that temperature at which $RO_2/R = 1$) using more recent thermochemical data. Their value of the ceiling temperature for $R = CH_3$ at 0.1 atm O_2 is 862 K, while the rate parameters in Table II provide a ceiling temperature for this equilibrium of 915 K. As noted earlier, this computationally determined ceiling temperature was based on the sensitivity of the computed rate of fuel consumption and the CH_4 and C_2H_6 yields to the equilibrium constant for reaction 101.

B. Test of the mechanism with independent experimental data

Also plotted as Curve C in Fig. 6 are the values of maximum reaction rate measured by Baldwin et al. [20] for mixtures with a composition of $CH_3CHO:O_2:N_2 = 2:30:28$, which were carried out at a constant pressure of 60 Torr throughout the temperature range. In their experiments, Baldwin et al. related the rate of reaction to the rate of pressure rise, measured in millimeters of Hg; over the temperature range studied $\Delta P \approx \Delta$acetaldehyde.

The mechanism in Table II was used to obtain model results for selected initial conditions studied by Baldwin et al. These calculated maximum rates of acetaldehyde consumption are plotted as Curve D in Figure 6. The predicted location of the negative temperature coefficient region agrees with that observed by Baldwin et al. The calculated maximum rates of acetaldehyde consumption also agree with Baldwin et al. at temperatures above about 740 K. However, between 600 K and 700 K, the predicted rate is considerably smaller than that measured. However, in this temperature region the rates (both measured and calculated) are very sensitive to the initial CH_3CHO concentration, increasing by a factor of 2 when the initial CH_3CHO is increased by 15%. Thus, comparisons of absolute rates near 813 K, where the sensitivity of the rate to initial concentration is much smaller, are probably more reliable. In Table III, product yields obtained by Baldwin et al. are compared with predicted yields. Again, the overall agreement is good, with the exception of the H_2 and H_2O_2 yields. The good agreement between measured and predicted methane and ethane yields provides additional evidence that the value of $K_{eq}(101)$ determined in our experiments is reliable.

The data of Baldwin et al. provide rates of formation of H_2, which were not determined in our experiments. In order to obtain the relatively high H_2 yields observed, the rate of reaction 87

$$CH_3O + M = CH_2O + H + M \qquad (87)$$

would need to be increased by a factor of 75 above the low pressure value [67] listed in Table II. The magnitude of this rate would then lie between the low pressure rate (5×10^{13} exp(-21000/RT)) and the high pressure limiting value (1.6×10^{14} exp(-27500/RT)) [68]. Even with such a rate increase, however, the model does not correctly predict the observed decrease in H_2 yield as the temperature increases. This may indicate that other reactions not included in the model contribute to hydrogen formation in this temperature regime.

Baldwin et al. [20] reported further measurements of product yields at a temperature of 813 K for a variety of initial pressures and compositions. These experiments were simulated numerically, using the present reaction mechanism. The computed product yields for these six cases are compared with the measured data in Table IV. Predicted yields of H_2O and H_2O_2, not presented by Baldwin et al., are also shown. For CH_4, CH_2O, CH_3OH, C_2H_6, and CO the overall agreement is very good, but the model predictions for CO_2 and H_2 yields are quite low. As already discussed, the predicted mechanism for H_2 production depends on a rapid source of H atoms which then abstract H atoms from acetaldehyde to produce H_2. The rate of the primary source of H atoms, reaction 87, is uncertain under present conditions and this may account in part for the low predicted yields of H_2. Both predicted and measured CO_2 yields are quite small and the disagreement between the two sets of small values is probably not important.

The satisfactory overall agreement of the model results with both the acetaldehyde consumption rate and the product yields obtained by Baldwin et al. lends support to the validity of the mechanism in Table II. It is evident that the experimental results are not severely affected by changes in surface-to-volume ratio, reactor geometry, or surface preparation since the data from two different experimental facilities seem to be consistent with each other.

In the undiluted, high O_2 cases and in the higher temperature cases of Baldwin et al., the early rates of reaction are very high (see Curve B of Fig. 2). As the temperature is increased above 600K, the computed time at which the maximum rate of reaction occurs is as short as 0.1 seconds after initiation. This time is much shorter than is observable in either the present experiments or those of Baldwin et al. and may contribute to experimental uncertainty in the observed maximum rate. In Fig. 6, all three sets of predictions for the maximum rate of fuel consumption have roughly the same shape, rising to a rather flat maximum, followed by a slight decrease from 650 K to 720-760 K, and then a rapid increase. However, in the Baldwin et al. experiments and in the present experiments as well, measurements of the rate of reaction were begun only after at least 2 seconds of reaction time. In the computer simulations, the rate of fuel consumption after 2 seconds can be considerably smaller that the actual maximum rate. For example, at 740 K on Curve B of Fig. 6, the computed maximum rate of acetaldehyde consumption is 6.95×10^{-9} moles/cm^3-sec, attained at a reaction time of 0.5 seconds. However, by the time the reaction has proceeded for 2 seconds, the rate of acetaldehyde consumption has fallen to 4.98×10^{-9} moles/cm^3-sec, a reduction of nearly 30%. Similar reductions of between 10% and 30% were computed for all of the mixtures over the temperature range of 710-750 K. Therefore, the measured maximum rates (as in Curve C of Fig. 6) will show a more pronounced local minimum in this temperature range than in the computed results because, in fact, the experiments are not able to observe the actual maximum rate.

C. Predicted product yields and radical concentrations

The variation in predicted product yields with temperature is illustrated in Fig. 7 for the low O_2 (diluted) case. These yields were evaluated at a time when approximately one-third of the CH_3CHO fuel had been consumed. The CO_2 and CH_3O_2H yields are appreciable at the lowest temperatures but decrease rapidly as the temperature is increased, effectively disappearing above about 600 K. The CO yield is consistently quite large over the entire range, and the CH_4 yield grows rapidly as the temperature increases above 650 K. Variations in methanol, formaldehyde, and water yields are also noted.

The corresponding radical species concentrations, again calculated after about one third of the acetaldehyde fuel has been consumed, are plotted in Fig. 8 for the diluted cases. The decrease in CH_3O_2 level is due to the temperature dependence of the equilibrium for Reaction 101 which drives the reaction to the left at higher temperatures as discussed earlier. The decrease in HO_2 also results from the reversal of this reaction, because the major source of HO_2 is the reaction of methoxy radicals with O_2, reaction 88. Methoxy radicals are produced both from CH_3O_2 at low temperatures (reactions 23, 24, and 26)and also by reaction of methyl radicals with HO_2 at higher temperatures. Under high temperature-low O_2 conditions, little CH_3O will be present because there will be little CH_3O_2 or HO_2 formed during the reaction. Above 800 K the principal radical species is CH_3, dominating HO_2, CH_3O, CH_3O_2, and CH_3CO_3, all of which were more important than CH_3 at lower temperatures.

The principal reactions consuming the acetaldehyde fuel vary with temperature, since the radical populations also vary. This is illustrated in Fig. 9, showing the fraction of the total acetaldehyde consumption rate that is contributed by reactions with the indicated radical species for the diluted (low initial O_2) mixtures. The populations of the abstracting radicals are controlled principally by the equilibria of Reactions 13 and 101. For example, as temperature increases, fewer methyl radicals combine with O_2 to make CH_3O_2 and CH_3O, so less acetaldehyde is consumed by these radicals in reactions forming mathanol and methylhydroperoxide. Instead, methyl radicals react with acetaldehyde to produce methane by Reaction 7, consistent with Figs. 7 and 8. Nearly all of the H_2O production results from reaction 4 between OH and acetaldehyde, and the OH curve in Fig. 9 is virtually identical to the H_2O curve in Fig. 7. The overall nature of the oxidation process similarly changes significantly as the temperature changes. As already noted, consumption of acetaldehyde by radicals such as CH_3O_2 and CH_3CO_3 leads to substantial chain branching. However, when CH_3, OH, or CH_3O react with the fuel, there is no branching, because the reaction products CH_4, H_2O, and CH_3OH are essentially unreactive. Therefore, the reaction rate slows as the temperature is increased in this regime because of the decreased branching.

Product yields in the undiluted (high O_2) cases are plotted as functions of temperature in Fig. 10. Comparison with the low O_2 results from Fig. 7 show that CO_2, H_2O, and CH_2O yields are higher and CH_4 and CH_3OH yields are lower in the high O_2 cases. These trends can be easily interpreted in terms of the influence of O_2 levels on the equilibria in Reactions 13 and 101 and the competition between reactions 9 and 88. As O_2 concentration is increased, the equilibrium shifts towards the adduct side of these reactions, and abstraction of H atoms from methoxy by O_2 to form CH_2O becomes more important. The CH_3 levels are therefore lowered, reducing the CH_4 yields, while the increased production of CO_2 results from the shift in the equilibrium of Reaction 13. Both addition steps lead to increased production of OH in the higher O_2 mixtures and therefore to higher production of H_2O. The radical species concentrations are shown in Fig. 11. It is interesting to note that the HO_2 and CH_3O_2 levels follow the negative temperature coefficient profile of Fig. 6. In contrast with the results plotted in Fig. 9, calculations show that the fastest reaction consuming acetaldehyde over the entire temperature range is Reaction 4 with OH, contributing more than 40% of the fuel consumption at all temperatures studied. At the lower temperatures, reactions of acetaldehyde with CH_3CO_3 and CH_3O also contribute significant fractions of the rate fuel consumption, while at 750 K and above, reactions with HO_2 and CH_3 are also important.

CONCLUSIONS

The proposed reaction mechanism provides a consistent description of the kinetics of acetaldehyde oxidation over the temperature range 550-900K. The present experimental results and those of Baldwin et al. [20] provide a demanding test of this mechanism, and most of the qualitative features and quantitative product yields measured in these experiments are reproduced by the model. This model predicts a region of negative temperature coefficient which coincides with that observed experimentally, and concentrations of radical and minor stable intermediate species, unavailable in the experiments, have been computed.

The keys to the oxidation mechanism, as determined from sensitivity analyses of the modeling results, were found to be the equilibria of the addition reactions of O_2 to CH_3 and CH_3CO, the competing oxidation reactions of the CH_3O_2 and CH_3O radicals, and the thermal decomposition of the acetyl radical. Other less important sensitivities of computed product species yields led to refinements in reaction rate parameters for H atom abstraction from acetaldehyde. All of these rate parameter modifications are reflected in the mechanism given in Table II.

The importance of the pressure dependent reactions 13 and 101 may have important implications with respect to the kinetic modeling of knock in internal combustion engines [22]. Under conditions where knock can occur, pressures can approach 30-40 atmospheres, higher than those of the present study by a factor of about 100. From the present modeling study, it might be expected that such an increase in pressure could shift the negative temperature coefficient regime to higher temperatures than those of Figure 6. Although acetaldehyde is not an engine fuel itself, it is formed in appreciable amounts during the combustion of practical fuels. More important, the same trends discussed here for the reactions of the methyl and acetyl radicals and the equilibria with the products of their addition reactions with O_2 will be valid for the radical species produced by other hydrocarbon fuels. Since the end gases subject to knock experience temperatures below 1000 K for a large fraction of the time of a typical engine combustion cycle, the present results indicate very strongly that it is essential to include the competitive addition reaction paths discussed above in any kinetic modeling study of engine knock.

ACKNOWLEDGMENTS

The authors appreciate prepublication results on $CH_3 + O_2$ addition reaction experiments and extended discussions with Professor David Gutman. The computational portion of this work was carried out under the auspices of the U.S. Department of Energy by the Lawrence Livermore National Laboratory under contract No. W-7405-ENG-48.

REFERENCES

1. By, A., Kempinski, B., and Rife, J.M., SAE Paper 810147, The Society of Automotive Engineers (1981).

2. Luck, C.J., Burgess, A.R., Desty, D.H., Whitehead, D.M., and Pratley, G., Fourteenth Symposium (International) on Combustion, p. 501, The Combustion Institute, Pittsburgh (1972).

3. Fish, A., Read, I.A., Affleck, W.S., and Haskell, W.W., Combust. Flame 13, 39 (1969).

4. Agnew, W.G., Twentieth Symposium (International) on Combustion, in press (1985).

5. Downs, D., Walsh, A.D., and Wheeler, R.W., Phil. Trans. Royal Soc. London A, 243, 463 (1951).

6. Felton, P.G., Gray, B.F., and Shank, N., Combust. Flame 27, 363 (1976).

7. Gray, P., Griffiths, J.F., Hasko, S.M., and Lignola, P.-G., Proc. Roy. Soc. (Lond) A374, 313 (1981).

8. Halstead, M.P., Prothero, A., and Quinn, C.P., Combust. Flame 20, 211 (1973).

9. Westbrook, C.K., and Dryer, F.L., Eighteenth Symposium (International) on Combustion, p. 749, The Combustion Institute, Pittsburgh (1981).

10. Kaiser, E.W., Int. J. Chem. Kinet. 15, 997 (1983).

11. Colket, M.B., Naegeli, D.W., and Glassman, I., Sixteenth Symposium (International) on Combustion, p. 1023, The Combustion Institute, Pittsburgh (1977).

12. Beeley, P., Griffiths, J.F., Hunt, B.A., and Williams, A., Sixteenth Symposium (International) on Combustion, p. 1013, The Combustion Institute, Pittsburgh (1977).

13. Gibson, C., Gray, P., Griffiths, J.F., and Hasko, S.M., Twentieth Symposium (International) on Combustion, in press (1985).

13a. Baldwin, R.R., and Mayor, L., Trans. Farad. Soc. 60, 80 (1960).

14. Benson, S.W., Prog. Energy Combust. Sci. 7, 125 (1981).

15. Lund, C.M., University of California Lawrence Livermore National Laboratory report UCRL-52504 (1978).

16. Pitz, W.J., Westbrook, C.K., Proscia, W.M., and Dryer, F.L., Twentieth Symposium (International) on Combustion, in press (1985).

17. JANAF Thermochemical Tables, D.R. Stull and H. Prophet, eds., NSRDS-NBS 37, National Bureau of Standards and Supplements.

18. Bahn, G.S., NASA report CR-2178 (1973).

19. Baldwin, R.R., Lewis, K.A., and Walker, R.W., Combust. Flame 34, 275 (1979).

20. Baldwin, R.R., Matchan, M.J., and Walker, R.W., Combust. Flame 15, 109 (1970).

21. Benson, S.W., J. Am Chem. Soc. 87, 972 (1965).

22. Pitz, W.J., and Westbrook, C.K., submitted for publication (1984).

23. Griffiths, J.F., and Hasko, S.M., Proc. Roy. Soc. Lond. A393, 371 (1984).

24. Warnatz, J., Eighteenth Symposium (International) on Combustion, p. 369, The Combustion Institute, Pittsburgh (1981).

25. Lin, M.T., and Laidler, K.J., Can. J. Chem. 46, 479 (1968).

26. Kelly, N., and Heicklen, J., J. Photochem. 8, 83 (1978).

27. Kerr, J.A., and Lloyd, A.C., Trans. Farad. Soc. 63, 2480 (1967).

28. McDade, C.E., Lenhardt, T.M., and Bayes, K.D., J. Photochem. 20, 1 (1982).

29. Benson, S.W., Oxid. Commun. 2, 169 (1982).

30. Addison, M.C., Burrows, J.P., Cox, R.A., and Patrick, R., Chem. Phys. Lett. 73, 283 (1980).

31. Cox, R.A., and Tyndall, G.S., J. Chem. Soc. Farad. II 76, 153 (1980).

32. Parkes, D.A., Int. J. Chem. Kinet. 9, 451 (1977).

33. Baldwin, R.R., and Walker, R.W., Combust. Flame 21, 55 (1973).

34. Selby, K., and Waddington, D.J., J. Chem. Soc. Perkin II, 1259 (1979).

35. Batt, L., and McCulloch, R.D., Int. J. Chem. Kinet. 8, 491 (1976).

36. Niki, H., Maker, P.D., Savage, C.M., and Breitenbach, L.P., J. Phys. Chem. 87, 2190 (1983).

37. Batt, L., Int. J. Chem. Kinet. 9, 977 (1979).

38. Batt, L., private communication, 1979.

39. Westbrook, C.K., and Dryer, F.L., Comb. Sci. Technol. 20, 125 (1979).

40. Aronowitz, D., Santoro, R.J., Dryer, F.L., and Glassman, I., Seventeenth Symposium (International) on Combustion, p. 633, The Combustion Institute, Pittsburgh, 1979.

41. Hagele, J., Lorenz, K., Rhasa, D., and Zellner, R., Ber. Bunsenges. Phys. Chem. 87, 1023 (1983).

42. Gray, P., and Herod, A.A., Trans. Farad. Soc. 64, 2723 (1968).

43. LeFevre, H.F., Meagher, J.F., and Timmons, R.B., Int. J. Chem. Kinet. 4, 103 (1972).

44. Wang, W.C., Suto, M., and Lee, L.C., J. Chem. Phys. 81, 3122 (1984).

45. Miller, J.A., J. Chem. Phys. 74, 5120 (1981).

46. Baulch, D.L., Drysdale, D.D., Horne, D.G., and Lloyd, A.C., Evaluated Kinetic Data for High Temperature Reactions, Butterworths, London, 1973.

47. Moretti, G., AIAA J. 3, 223 (1965).

48. Jenkins, D.R., Yumlu, V.S., and Spalding, D.B., Eleventh Symposium (International) on Combustion, p. 779, The Combustion Institute, Pittsburgh, 1967.

49. Lloyd, A.C., Int. J. Chem. Kinet. 6, 169 (1974).

50. Kircher, C.C., and Sander, S.P., J. Phys. Chem. 88, 2082 (1984).

51. Baulch, D.L., and Drysdale, D.D., Combust. Flame 23, 215 (1974).

52. Baulch, D.L., Drysdale, D.D., Duxbury, J., and Grant, S., Evaluated Kinetic Data for High Temperature Reactions, vol. 3, Butterworths, London, 1976.

53. Gardiner, W.C., Jr., McFarland, M., Morinaga, K., Takeyama, T., and Walker, B.F., J. Phys. Chem. 75, 1504 (1971).

54. Simonaitis, R., and Heicklen, J., J. Chem. Phys. 56, 2004 (1972).

55. Westbrook, C.K., Creighton, J., Lund, C., and Dryer, F.L., J. Phys. Chem. 81, 2542 (1977).

56. Langford, A.O., and Moore, C.B., J. Chem. Phys. 80, 4211 (1984).

57. Niki, H., Daby, E.E., and Weinstock, B., Twelfth Symposium (International) on Combustion, p. 277, The Combustion Institute, Pittsburgh, 1969.

58. Westenberg, A.A., and de Haas, N., J. Phys. Chem. 76, 2215 (1972).

59. Tunder, R., Mayer, S., Cook, E., and Schieler, L., Aerospace Corp. report TR-1001 (9210-02)-1 (AD813485), 1966.

60. Baldwin, R.R., and Walker, R.W., Fourteenth Symposium (International) on Combustion, p. 241, The Combustion Institute, Pittsburgh, 1973.

61. Bowman, C.T., Combust. Sci. Technol. 2, 161 (1970).

62. Dean, A.M., Johnson, R.L., and Steiner, D.C., Combust. Flame 37, 41 (1980).

63. Atkinson, R., and Pitts, J.N., J. Chem. Phys. 68, 3581 (1978).

64. Bowman, C.T., Fifteenth Symposium (International) on Combustion, p. 869, The Combustion Institute, Pittsburgh, 1975.

65. Baldwin, R.R., and Walker, R.W., Seventeenth Symposium (International) on Combustion, p. 525, The Combustion Institute, Pittsburgh, 1979.

66. Manthorne, K.C., and Pacey, P.D., Can. J. Chem. 56, 1307 (1978).

67. Brabbs, T.A., and Brokaw, R.S., Fifteenth Symposium (International) on Combustion, p. 893, The Combustion Institute, Pittsburgh, 1975.

68. Batt, L., Int. J. Chem. Kinet. 11, 977 (1979).

69. Cox, R.A., Derwent, R.G., Kearsey, S.V., Batt, L., and Patrick, K.G., J. Photochem. 13, 149 (1980).

70. Gutman, D., Sanders, N., and Butler, J.E., J. Phys. Chem. 86, 66 (1982).

71. Pitz, W.J., Westbrook, C.K., Proscia, W.M., and Dryer, F.L., Twentieth Symposium (International) on Combustion, in press (1985).

72. Hartig, R., Troe, J., and Wagner, H.Gg., Thirteenth Symposium (International) on Combustion, p. 147, The Combustion Institute, Pittsburgh, 1971.

73. Baldwin, R.R., Hopkins, D.E., Norris, A.C., and Walker, R.W., Combustion and Flame 15, 33 (1970).

74. Tully, F.P., and Ravishankara, A.R., J. Phys. Chem. 84, 3126 (1980).

75. Michael, J.V., Keil, D.G., and Klemm, R.B., Int. J. Chem. Kinet. 15, 705 (1983).

76. Skinner, G.B., Lifshitz, A., Scheller, K., and Burcat, A., J. Chem. Phys. 56, 3853 (1972).

77. Fenimore, C.P., Twelfth Symposium (International) on Combustion, p. 463, The Combustion Institute, Pittsburgh, 1969.

78. Peeters, J., and Mahnen, G., Fourteenth Symposium (International) on Combustion, p. 133, The Combustion Institute, Pittsburgh, 1973.

79. Baulch, D.L., and Duxbury, J., Combust. Flame 37, 313 (1980).

80. Warnatz, J., Combustion Science and Technology 34, 177 (1983).

81. Notzold, D., and Algermissen, J., Combustion and Flame 40, 293 (1981).

82. Clark, T.C., and Dove, J.E., Canad. J. Chem. 51, 2147 (1973).

83. Tully, F.P., Ravishankara, A.R., and Carr, K., Int. J. Chem. Kinet. 15, 1111 (1983).

84. Tanzawa, T., and Klemm, R.B., paper presented at the 179th National Meeting of the American Chemical Society, Houston, Texas, 1980.

85. Baldwin, R.R., Bennett, J.P., and Walker, R.W., Sixteenth Symposium (International) on Combustion, p. 1041, The Combustion Institute, Pittsburgh, 1977.

86. Allara, D.L., and Shaw, R., J. Phys. Chem. Ref. Data 9, 523 (1980).

87. Olson, D.B., Tanzawa, T., and Gardiner, W.C., Jr., Int. J. Chem. Kinet. 11, 23 (1979).

88. Westbrook, C.K., Combustion Science and Technology 20, 5 (1979).

89. Benson, S.W., and Haugen, G.R., J. Phys. Chem. 71, 1735 (1967).

90. Westbrook, C.K., Dryer, F.L., and Schug, K.P., Nineteenth Symposium (International) on Combustion, p. 153, The Combustion Institute, Pittsburgh, 1983.

91. Davis, D.D., Huie, R.E., Kurylo, M.J., and Braun, W., J. Chem. Phys. 56, 4868 (1972).

92. Tanzawa, T., and Gardiner, W.C., Jr., Combust. and Flame 39, 241 (1980).

93. Jachimowski, C.J., Combustion and Flame 29, 55 (1977).

94. Gardiner, W.C., Jr., and Walker, B.F., J. Chem. Phys. 48, 5279 (1968).

95. Browne, W.G., Porter, R.P., Verlin, J.D., and Clark, A.H., Twelfth Symposium (International) on Combustion, p. 1035, The Combustion Institute, Pittsburgh, 1969.

96. Vandooren, J., and van Tiggelen, P.J., Sixteenth Symposium (International) on Combustion, p. 1133, The Combustion Institute, Pittsburgh, 1977.

97. Miller, J.A., Mitchell, R.E., Smooke, M.D., and Kee, R.J., Nineteenth Symposium (International) on Combustion, p. 181, The Combustion Institute, Pittsburgh, 1983.

98. Michael, J.V., Nava, D.F., Payne, W.A., and Stief, L.J., J. Chem. Phys. 70, 5222.

99. Warnatz, J., Eighteenth Symposium (International) on Combustion, p. 369, The Combustion Institute, Pittsburgh, 1981.

100. Peeters, J., and Mahnen, G., Combustion Institute European Symposium, p. 53, 1973.

101. Mayer, S.W., Schieler, L., and Johnston, H.S., Eleventh Symposium (International) on Combustion, p. 837, The Combustion Institute, Pittsburgh, 1967.

102. Peeters, J., and Vinckier, C., Fifteenth Symposium (International) on Combustion, p. 969, The Combustion Institute, Pittsburgh, 1975.

103. Khachatryan, L.A., Niazyan, O.M., Mantashyan, A.A., Vedeneev, V.I., and Teitel'boim, M.A., Int. J. Chem. Kinet. 14, 1231 (1982).

104. Morgan, C.A., Pilling, M.J., Tulloch, J.M., Ruiz, R.P., and Bayes, K., J. Chem. Soc., Faraday Trans. 2, 78, 1323 (1982).

105. McDowell, C.A., and Sharples, L.K., Canad. J. Chem. 36, 251 (1958).

106. Pratt, G.L., and Wood, S.W., J. Chem. Soc. Farad. Trans. I 80, 3419 (1984).

107. Watkins, K.W., and Word, W.W., Int. J. Chem. Kinet. 6, 855 (1974).

108. Slagle, I.R., Feng, Q., and Gutman, D., J. Phys. Chem. 88, 3648 (1984).

109. Slagle, I.R., Park, J.-Y., and Gutman, D., Twentieth Symposium (international) on Combustion, in pressf (1985).

110. O'Neal, E., and Benson, S.W., J. Chem. Phys. 36, 2196 (1962).

111. Kondo, O., and Benson, S.W., J. Chem. Phys. 88, 6675 (1984).

112. Slagle, I.R., and Gutman, D., submitted for publication (1985).

113. Gutman, D., personal communication.

114. Benson, S.W., Thermochemical Kinetics, Wiley, New York, 1976.

115. Kirk, A.D., and Knox, J.H., Trans. Farad. Soc. 56, 1296 (1960).

Table I

Product densities at 713 K

Species	Product density (molecules/cm^3 x 10^{-16})	
	Experiment	Model
CH_4	0.15	0.13
C_2H_6	0.006	0.002
CH_3OH	0.56	0.49
CH_2O	1.39	1.35
CO	2.94	3.24
CO_2	0.15	0.15
H_2O	1.5 - 3.0[a]	1.3
H_2O_2	0.7	1.47

[a] The water concentration was uncertain because of the relatively high H_2O_2 yield. The H_2O_2 mass spectrum contains a mass fragment at 18 amu which interferes with the H_2O determination.

Initial concentrations: $CH_3CHO = 4.5x10^{16}$; $O_2 = 8x10^{17}$; $A=N_2=0$ molecules/cm^3.

The measured product yields were obtained after 15 seconds of reaction time when $2.6x10^{16}$ molecules/cm^3 of CH_3CHO had been consumed.

Table II

Reaction mechanism for acetaldehyde oxidation
Reaction rates are in cm^3-mole-sec-kcal units, $k=AT^n\exp(-E_a/RT)$

		Forward rate			Reverse rate			Ref
	Reaction	log A	n	E_a	log A	n	E_a	
1	$CH_3CHO = CH_3+HCO$	15.85	0	81.78	9.58	1	0.00	[11]
2	$CH_3CHO+O_2 = CH_3CO+HO_2$	13.30	0.5	42.20	7.00	0.5	4.00	[11]
3	$CH_3CHO+H = CH_3CO+H_2$	13.60	0	4.20	13.25	0	23.67	[24]
4	$CH_3CHO+OH = CH_3CO+H_2O$	13.00	0	0.00	13.28	0	36.62	[24,a]
5	$CH_3CHO+O = CH_3CO+OH$	12.70	0	1.79	12.00	0	19.16	[24]
6	$CH_3CHO+HO_2 = CH_3CO+H_2O_2$	12.23	0	10.70	12.00	0	14.10	[11]
7	$CH_3CHO+CH_3 = CH_3CO+CH_4$	12.24	0	8.44	13.18	0	28.00	[25]
8	$CH_3CHO+CH_3CO_3 = CH_3CO+CH_3CO_3H$	11.08	0	4.90	10.30	0	10.00	[105;a,b
9	$CH_3CHO+CH_3O = CH_3CO+CH_3OH$	11.06	0	1.28	11.48	0	18.16	[26,a,b]
10	$CH_3CHO+CH_3O_2 = CH_3CO+CH_3O_2H$	9.55	0	5.05	9.70	0	10.10	a,c
11	$CH_3CHO+C_2H_5O_2 = CH_3CO+C_2H_5O_2H$	9.55	0	5.05	9.70	0	10.10	d
12	$CH_3CO+M = CH_3+CO+M$	16.26	0	14.40	11.20	0	5.97	e
13	$CH_3CO+O_2 = CH_3CO_3$	10.00	0	-2.70	16.46	-1	37.30	[28,g,y]
14	$CH_3CO_3+HO_2 = CH_3CO_3H+O_2$	12.00	0	0.00	*			f
15	$CH_3CO_3H = CH_3CO_2+OH$	15.60	0	40.00	*			[29]
16	$CH_3CO_3H = CH_3+CO_2+OH$	14.30	0	40.15	*			f
17	$CH_3CO_3+CH_3O_2 = CH_3CO_2+CH_3O+O_2$	12.26	0	0.00	*			[30,g]
18	$CH_3CO_3+CH_3O_2 = CH_3CO_2H+CH_2O+O_2$	11.48	0	0.00	*			f,h
19	$CH_3CO_3+HO_2 = CH_3CO_2+OH+O_2$	12.00	0	0.00	*			f,i
20	$CH_3CO_3+CH_3CO_3 = CH_3CO_2+CH_3CO_2+O_2$	12.26	0	0.00	*			[30,j]
21	$CH_3CO_2+M = CH_3+CO_2+M$	16.26	0	14.40	*			[30,j]
22	$CH_3O_2+HO_2 = CH_3O_2H+O_2$	10.66	0	-2.60	12.48	0	39.00	[31]
23	$CH_3O_2+CH_3 = CH_3O+CH_3O$	12.95	0	0.00	10.30	0	0.00	[32,a]
24	$CH_3O_2+HO_2 = CH_3O+OH+O_2$	12.00	0	0.00	*			[33,k]
25	$CH_3O_2+CH_3O_2 = CH_2O+CH_3OH+O_2$	11.26	0	0.00	*			l
26	$CH_3O_2+CH_3O_2 = CH_3O+CH_3O+O_2$	12.57	0	2.20	*			l
27	$CH_3O_2+CH_3O_2 = CH_3O_2CH_3+O_2$	11.70	0	2.00	*			l
28	$CH_3O_2CH_3 = CH_3O+CH_3O$	15.48	0	37.00	*			[35]
29	$CH_3O_2H = CH_3O+OH$	14.81	0	43.00	13.53	1	34.57	m
30	$CH_3O_2H+OH = CH_3O_2+H_2O$	13.51	0	1.00	13.48	0	32.80	[36]
31	$CH_3O_2H+OH = CH_2O_2H+H_2O$	13.40	0	1.00	13.48	0	32.80	[36]
32	$CH_3O_2H+CH_3O = CH_3O_2+CH_3OH$	11.85	0	4.00	13.48	0	32.80	f
33	$CH_3O_2H+CH_3O = CH_2O_2H+CH_3OH$	11.85	0	4.00	13.48	0	32.80	f
34	$C_2H_5O_2+HO_2 = C_2H_5O_2H+O_2$	10.66	0	-2.60	12.48	0	39.00	n
35	$C_2H_5O_2+HO_2 = C_2H_5O+OH+O_2$	12.00	0	0.00	*			[33]
36	$C_2H_5O_2H = C_2H_5O+OH$	14.81	0	43.00	13.53	1	34.57	o
37	$C_2H_5O = CH_3+CH_2O$	15.00	0	21.60	5.30	1	9.82	[37]
38	$C_2H_5O+O_2 = CH_3CHO+HO_2$	12.70	0	4.00	11.11	0	32.17	[33,38]
39	$CH_3OH+M = CH_3+OH+M$	18.48	0	80.00	13.16	1	-10.98	[39]
40	$CH_3OH+HO_2 = CH_2OH+H_2O_2$	12.80	0	19.36	7.00	1.66	11.44	[40]
41	$CH_3OH+OH = CH_2OH+H_2O$	12.60	0	1.37	7.27	1.66	24.68	[41]
42	$CH_3OH+H = CH_2OH+H_2$	13.48	0	7.00	7.51	1.66	15.16	[39]
43	$CH_3OH+H = CH_3+H_2O$	12.72	0	5.34	12.32	0	36.95	[39]
44	$CH_3OH+CH_3 = CH_2OH+CH_4$	11.26	0	9.80	6.70	1.66	18.43	[42]
45	$CH_3OH+O = CH_2OH+OH$	12.23	0	2.29	5.90	1.66	8.35	[43]
46	$CH_3OH+CH_3O = CH_2OH+CH_3OH$	12.18	0	7.00	5.34	1.66	10.85	p
47	$CH_3OH+OH = CH_3O+H_2O$	13.09	0	3.25	13.50	0	21.46	[41]
48	$CH_2OH+M = CH_2O+H+M$	13.40	0	29.00	16.69	-0.66	7.58	[39]
49	$CH_2OH+O_2 = CH_2O+HO_2$	11.92	0	0.00	17.86	-1.66	22.32	[44]

Table II (continued)

Reaction mechanism for acetaldehyde oxidation
Reaction rates are in cm^3-mole-sec-kcal units, $k = AT^n \exp(-E_a/RT)$

		Forward rate			Reverse rate			Ref
	Reaction	log A	n	E_a	log A	n	E_a	
50	$H+O_2 = O+OH$	16.71	-0.82	16.51	13.12	0	0.68	[45]
51	$H_2+O = H+OH$	10.26	1	8.90	9.92	1	6.95	[46]
52	$O+H_2O = OH+OH$	13.83	0	18.35	12.80	0	1.10	[46]
53	$H_2+OH = H_2O+H$	13.34	0	5.15	13.98	0	20.30	[46]
54	$H+O_2+M = HO_2+M$	15.22	0	-1.00	15.36	0	45.90	[46]
55	$H_2O+M = H+OH+M$	16.34	0	105.00	23.15	-2	0.00	[46]
56	$OH+M = O+H+M$	19.90	-1	103.70	16.00	0	0.00	[47]
57	$O_2+M = O+O+M$	15.71	0	115.00	15.67	-0.28	0.00	[48]
58	$H_2+M = H+H+M$	14.34	0	96.00	15.48	0	0.00	[46]
59	$HO_2+O = OH+O_2$	13.70	0	1.00	13.81	0	56.61	[49]
60	$HO_2+H = OH+OH$	14.40	0	1.90	13.08	0	40.10	[46]
61	$HO_2+H = H_2+O_2$	13.40	0	0.70	13.74	0	57.80	[46]
62	$HO_2+OH = H_2O+O_2$	13.70	0	1.00	14.80	0	73.86	[49]
63	$HO_2+HO_2 = H_2O_2+O_2$	11.11	0	-1.24	13.60	0	42.64	[50]
64	$H_2O_2+OH = H_2O+HO_2$	13.00	0	1.80	13.45	0	32.79	[46]
65	$H_2O_2+H = HO_2+H_2$	12.23	0	3.75	11.86	0	18.70	[46]
66	$H_2O_2+M = OH+OH+M$	17.08	0	45.50	14.96	0	-5.07	[46]
67	$CO+OH = CO_2+H$	7.18	1.3	-0.77	9.23	1.3	21.58	[51]
68	$CO+HO_2 = CO_2+OH$	14.18	0	23.65	15.23	0	85.50	[52]
69	$CO+O_2 = CO_2+O$	11.50	0	37.60	12.44	0	43.83	[53]
70	$CO+O+M = CO_2+M$	15.77	0	4.10	21.74	-1	131.80	[54]
71	$HCO+M = H+CO+M$	14.16	0	19.00	11.70	1	1.55	[55]
72	$HCO+O_2 = CO+HO_2$	12.48	0	0.00	12.95	0	39.29	[56]
73	$HCO+H = CO+H_2$	14.30	0	0.00	15.12	0	90.00	[57]
74	$HCO+O = CO+OH$	14.00	0	0.00	14.46	0	87.90	[58]
75	$HCO+CH_3 = CO+CH_4$	11.48	0.5	0.00	13.71	0.5	90.47	[59]
76	$HCO+HO_2 = CH_2O+O_2$	14.00	0	3.00	15.56	0	46.04	[60]
77	$HCO+OH = CO+H_2O$	14.00	0	0.00	15.45	0	105.10	[61]
78	$CH_2O+M = HCO+H+M$	16.52	0	81.00	11.15	1	-11.77	[62]
79	$CH_2O+OH = HCO+H_2O$	12.88	0	0.17	12.41	0	30.00	[63]
80	$CH_2O+H = HCO+H_2$	14.52	0	10.50	13.42	0	25.17	[62]
81	$CH_2O+O = HCO+OH$	13.70	0	4.60	12.24	0	17.17	[64]
82	$CH_2O+HO_2 = HCO+H_2O_2$	11.30	0	8.00	10.34	0	6.59	[49,q]
83	$CH_2O+CH_3O = HCO+CH_3OH$	11.78	0	3.30	8.47	0	13.37	r
84	$CH_2O+CH_3O_2 = HCO+CH_3O_2H$	11.11	0	9.00	10.40	0	10.10	[29,s]
85	$CH_2O+C_2H_5O_2 = HCO+C_2H_5O_2H$	11.11	0	9.00	10.40	0	10.10	[29,s]
86	$CH_2O+CH_3 = HCO+CH_4$	10.00	0.5	6.00	10.32	0.5	21.14	[59,t]
87	$CH_3O+M = CH_2O+H+M$	13.70	0	21.00	9.00	1	-2.56	[67,u]
88	$CH_3O+O_2 = CH_2O+HO_2$	10.88	0	2.70	11.11	0	32.17	[69,v]
89	$CH_3O+CH_3O = CH_3OH+CH_2O$	13.48	0	0.00	12.19	0	79.57	[71]
90	$CH_4+M = CH_3+H+M$	17.15	0	88.40	11.45	1	-19.51	[72]
91	$CH_4+H = CH_3+H_2$	14.10	0	11.90	12.68	0	11.43	[73]
92	$CH_4+OH = CH_3+H_2O$	6.20	2.1	2.46	5.42	2.1	17.14	[74]
93	$CH_4+O = CH_3+OH$	6.33	2.2	6.48	4.55	2.2	3.92	[75]
94	$CH_4+HO_2 = CH_3+H_2O_2$	13.30	0	18.00	11.50	0	8.00	[76]
95	$CH_4+CH_3O = CH_3+CH_3OH$	11.30	0	7.00	9.02	0	2.22	[71]

Table II (continued)

Reaction mechanism for acetaldehyde oxidation
Reaction rates are in cm^3-mole-sec-kcal units, $k=AT^n\exp(-E_a/RT)$

	Reaction	Forward rate			Reverse rate			Ref
		log A	n	E_a	log A	n	E_a	
96	$CH_3+OH = CH_2O+H_2$	12.60	0	0.00	14.08	0	71.72	[77]
97	$CH_3+O = CH_2O+H$	14.11	0	2.00	15.23	0	71.63	[78]
98	$CH_3+O_2 = CH_3O+O$	13.68	0	29.00	14.48	0	0.73	[67]
99	$CH_3+HO_2 = CH_4+O_2$	12.00	0	0.40	13.88	0	58.59	[76]
100	$CH_3+HO_2 = CH_3O+OH$	13.51	0	0.00	10.30	0	0.00	[11]
101	$CH_3+O_2+M = CH_3O_2+M$	16.15	0	-1.10	16.86	0	26.53	[103,106]
102	$C_2H_6 = CH_3+CH_3$	19.35	-1	88.31	13.38	0	0.00	w
103	$C_2H_6+O_2 = C_2H_5+HO_2$	13.00	0	51.00	12.37	0	2.00	[81]
104	$C_2H_6+H = C_2H_5+H_2$	2.73	3.5	5.20	2.99	3.5	27.32	[82]
105	$C_2H_6+OH = C_2H_5+H_2O$	9.94	1.1	1.81	10.23	1.1	23.93	[83]
106	$C_2H_6+O = C_2H_5+OH$	14.05	0	7.85	13.32	0	12.72	[75,84]
107	$C_2H_6+HO_2 = C_2H_5+H_2O_2$	12.78	0	19.00	12.53	0	9.89	[85]
108	$C_2H_6+C_2H_4 = C_2H_5+C_2H_5$	11.70	0	60.00	11.70	0	0.00	[86]
109	$C_2H_6+CH_3O = C_2H_5+CH_3OH$	11.48	0	7.00	10.23	0	9.67	[29]
110	$C_2H_6+CH_3 = C_2H_5+CH_4$	-0.26	4	8.28	10.48	0	12.50	[82]
111	$C_2H_5+M = C_2H_4+H+M$	15.30	0	30.00	10.62	0	-11.03	[87]
112	$C_2H_5+O_2 = C_2H_4+HO_2$	12.00	0	5.00	11.12	0	13.70	[88]
113	$C_2H_5+CH_3 = C_2H_4+CH_4$	11.90	0	0.00	12.91	0	66.89	[86]
114	$C_2H_5+O_2 = C_2H_5O_2$	12.00	0	0.00	16.78	-1	31.20	[29]
115	$C_2H_5+C_2H_3 = C_2H_4+C_2H_4$	12.48	0	0.00	14.70	0	64.70	[89]
116	$C_2H_4+M = C_2H_2+H_2+M$	16.97	0	77.20	12.66	1	36.52	[90]
117	$C_2H_4+M = C_2H_3+H+M$	18.80	0	108.70	17.30	0	0.00	[90]
118	$C_2H_4+H = C_2H_3+H_2$	7.18	2	6.00	6.24	2	5.11	[90]
119	$C_2H_4+OH = C_2H_3+H_2O$	12.68	0	1.23	12.08	0	14.00	[90]
120	$C_2H_4+O = CH_2O+CH_2$	13.40	0	5.00	12.48	0	15.68	[90]
121	$C_2H_4+OH = CH_2O+CH_3$	12.30	0	0.96	11.78	0	16.48	[90]
122	$C_2H_4+O = CH_3+HCO$	12.52	0	1.13	11.20	0	31.18	[91]
123	$C_2H_3+M = C_2H_2+H+M$	14.90	0	31.50	11.09	1	-10.36	[89]
124	$C_2H_3+O_2 = C_2H_2+HO_2$	12.00	0	10.00	12.00	0	17.87	[90]
125	$C_2H_3+CH_3 = C_2H_2+CH_4$	11.90	0	0.00	13.78	0	66.05	x
126	$C_2H_3+H = C_2H_2+H_2$	13.30	0	2.50	13.12	0	68.08	[92]
127	$C_2H_2+M = C_2H+H+M$	14.00	0	114.00	9.04	1	0.77	[93]
128	$C_2H_2+O_2 = HCO+HCO$	12.60	0	28.00	11.00	0	63.65	[94]
129	$C_2H_2+H = C_2H+H_2$	14.30	0	19.00	13.62	0	13.21	[95]
130	$C_2H_2+OH = C_2H+H_2O$	12.78	0	7.00	12.73	0	16.36	[96]
131	$C_2H_2+O = C_2H+OH$	15.50	-0.6	17.00	14.47	-0.6	0.91	[95]
132	$C_2H_2+O = CH_2+CO$	13.83	0	4.00	13.10	0	54.67	[96]
133	$C_2H_2+O = HCCO+H$	4.55	2.7	1.39	2.70	2.7	12.79	[97]
134	$C_2H_2+OH = CH_2CO+H$	11.50	0	0.20	12.50	0	20.87	[96]
135	$CH_2CO+H = CH_3+CO$	13.04	0	3.40	12.38	0	40.20	[98]
136	$CH_2CO+O = HCO+HCO$	13.00	0	2.40	11.54	0	33.50	[99]
137	$CH_2CO+OH = CH_2+HCO$	13.45	0	0.00	13.44	0	18.50	[99]
138	$CH_2CO+M = CH_2+CO+M$	16.30	0	60.00	10.66	0	0.00	[97]
139	$CH_2CO+O = HCCO+OH$	13.70	0	8.00	10.85	0	8.00	[97]
140	$CH_2CO+OH = HCCO+H_2O$	12.88	0	3.00	11.03	0	11.00	[97]
141	$CH_2CO+H = HCCO+H_2$	13.88	0	8.00	11.39	0	8.00	[97]

Table II (continued)

Reaction mechanism for acetaldehyde oxidation
Reaction rates are in cm^3-mole-sec-kcal units, $k=AT^n\exp(-E_a/RT)$

		Forward rate			Reverse rate			Ref
	Reaction	log A	n	E_a	log A	n	E_a	
142	HCCO+OH = HCO+HCO	13.00	0	0.00	13.68	0	40.36	[97]
143	HCCO+H = CH_2+CO	13.70	0	0.00	13.82	0	39.26	[97]
144	HCCO+O = HCO+CO	13.53	0	2.00	13.92	0	128.30	[97]
145	C_2H+O_2 = HCO+CO	13.00	0	7.00	12.93	0	138.40	[95]
146	C_2H+O = CO+CH	13.70	0	0.00	13.50	0	59.43	[95]
147	CH_2+O_2 = HCO+OH	14.00	0	3.70	13.61	0	76.58	[100]
148	CH_2+O = CH+OH	11.28	0.7	25.00	10.77	0.7	25.93	[101]
149	CH_2+H = $CH+H_2$	11.43	0.7	25.70	11.28	0.7	28.73	[101]
150	CH_2+OH = $CH+H_2O$	11.43	0.7	25.70	11.91	0.7	43.88	[102]
151	$CH+O_2$ = CO+OH	11.13	0.7	25.70	11.71	0.7	185.60	[102]
152	$CH+O_2$ = HCO+O	13.00	0	0.00	13.13	0	71.95	[93]
153	CH_2O_2H = CH_2O+OH	15.60	0	23.00	13.50	1	14.57	f

---

* no reverse rate included
a Rate adjusted to fit experimental data
b Room temperature rate combined to estimate E_a (see text)
c Originally assumed equal to rate of Reaction 84
d Assumed equal to rate of Reaction 10
e Low pressure value estimated from high pressure measurements [107]
f Estimated
g Room temperature measurement with negative activation energy adjusted to fit observed CO/CO_2 ratio and overall rate (see text)
h Assumed approximately equal to rate of Reaction 25
i Assumed equal to rate of Reaction 24
j Sum of rates of Reactions 20 and 21 equal to value from Ref [30]
Rate of reaction 21 assumed equal to rate of Reaction 12
k Assumed equal to rate of analogous reaction of $C_2H_5O_2$ at 298 K [33]
l Sum of reactions 25, 26 and 27 agrees with Parkes [32].
$E_{25}-E_{26}$ taken from ref [34]
m See Appendix
n Assumed equal to rate of Reaction 22
o Assumed equal to rate of Reaction 29
p Assumed equal to rate of Reaction 95
q Based originally on Lloyd [49], then adjusted to fit data. Rate shown agrees well with Baldwin and Walker [65]
r Assumed equal to rate of Reaction 9
s Given rate is in reasonable agreement with ref [34]
t Given rate is in reasonable agreement with ref [66]
u See also ref [68]
v See also ref [70]
w High pressure limiting expression determined from reverse reaction rate [79] used at 553 K. Adjusted for falloff [80] at 713 K.
x Assumed equal to rate of Reaction 113
y Reverse rate calculated from thermochemistry in [14].

Table III

Comparison of Reaction Products at 713 K and 813 K
between experimental and computed results
Experimental data are from Baldwin et al. [20]
after consumption of 10% of the initial acetaldehyde

Temperature		713 K		813 K	
Initial pressure, mm Hg, of:	CH_3CHO	1.5		2.0	
	O_2	30.0		30.0	
	N_2	28.5		28.0	
Product yield, expressed as a percentage of the aldehyde consumed:		expmt.	comp.	expmt.	comp.
	CO_2	-	2.6	0.7	0.2
	CO	≈100	98	83	99
	CH_2O	65	65	32	29
	CH_4	10	8.5	50	49
	C_2H_6	0.5	0.2	6	3.9
	CH_3OH	25	20	7	12
	H_2O_2	10	37	5	11
	H_2	15	0.2	7	0.4
	H_2O	-	34	-	17

Table IV

Comparison between experimental product yields [20]
and computed results, evaluated at 10% fuel consumption

Initial temperature is 813 K in all cases

		Mixture					
Initial Mixture, mm Hg		1	2	3	4	5	6
CH_3CHO		0.5	2.0	8.0	2.0	0.5	4.0
O_2		30.0	30.0	30.0	3.0	7.5	60.0
N_2		29.5	28.0	22.0	55.0	7.0	56.0
Reaction Products, percentage of CH_3CHO consumed							
CH_4	a)	46.0	49.0	61.0	83.0	60.0	41.0
	b)	33.0	49.0	58.0	91.0	76.0	32.0
CH_2O	a)	39.0	32.0	20.0	7.5	26.0	39.0
	b)	50.0	29.0	11.0	0.5	8.8	44.0
CH_3OH	a)	4.0	7.2	10.0	4.6	8.0	10.0
	b)	5.1	10.6	15.0	1.3	3.1	16.0
C_2H_6	a)	5.4	5.8	4.3	2.2	3.1	4.6
	b)	4.3	3.9	3.2	2.3	5.5	2.4
CO	a)	108.0	83.0	93.0	98.0	94.0	107.0
	b)	102.0	99.0	91.0	97.0	99.0	101.0
CO_2	a)	2.5	0.7	1.6	1.4	0.5	1.8
	b)	0.1	0.2	0.3	0.1	0.1	0.3
H_2	a)	12.5	7.2	5.3	2.8	11.2	11.5
	b)	0.7	0.4	0.2	0.1	0.1	0.6
H_2O	b)	35.4	16.7	7.0	1.9	7.1	24.0
H_2O_2	b)	23.3	17.6	7.9	0.9	7.7	24.8

---

a) Experimental value
b) Calculated value

FIGURE CAPTIONS

1. Concentration-time profiles of CH_3CHO at 553 K. Initial conditions for the solid curve: $CH_3CHO = 4.7 \times 10^{16}$; $O_2 = 7.1 \times 10^{16}$; N_2 (or Ar) = 7.6×10^{17} molecules/cm^3. Initial conditions for the dashed curve: $CH_3CHO = 4.7 \times 10^{16}$; $O_2 = 8.35 \times 10^{17}$ molecules/cm^3 ; N_2 (or Ar) = 0.0. Individual symbols represent values predicted using the numerical model.

2. Concentration-time profiles of CH_3CHO at 713 K. Initial conditions for the solid curve: $CH_3CHO = 4.52 \times 10^{16}$; $O_2 = 6.77 \times 10^{16}$; N_2 (or Ar) = 7.33×10^{17} molecules/cm^3. Initial conditions for the dashed curve: $CH_3CHO = 4.52 \times 10^{16}$; $O_2 = 8.0 \times 10^{17}$ molecules/cm^3 ; N_2 (or Ar) = 0.0. Individual symbols represent values predicted using the numerical model.

3a. Product yields for low initial O_2 concentration (diluted)
3b. experiments at 553 K. Same initial conditions as Fig. 1, solid curve. Individual symbols represent computed values.

4a. Product yields for low initial O_2 concentration (diluted)
4b. experiments at 713 K. Same initial conditions as Fig. 2, solid curve. Individual symbols represent computed values.

5a. Product yields for high initial O_2 concentration (undiluted)
5b. experiments at 553 K. Same initial conditions as Fig. 1, dashed curve. Individual symbols represent computed values. The predicted ethane yield is 1×10^{-5}; the upper limit to the measured ethane yield is 5×10^{-5} per acetaldehyde consumed.

6. Computed results for maximum rate of acetaldehyde consumption in (A) low initial O_2 concentration and (B) high initial O_2 concentration mixtures. Curve C represents experimental results of Baldwin et al. [20]. Curve D shows calculated maximum rates using the reaction mechanism in Table II and the initial conditions of Baldwin et al. ($CH_3CHO:O_2:N_2=2:30:28$ at a total pressure of 60 torr).

7. Computed product species yields in low initial O_2 concentration cases.

8. Computed radical species yields in low initial O_2 concentration cases.

9. Reactions consuming acetaldehyde in low initial O_2 concentration cases, showing abstracting radical species and the fraction of the total acetaldehyde consumption contributed by reactions with that radical.

10. Computed product species yields in high initial O_2 concentration cases.

11. Computed radical species yields in high initial O_2 concentration cases.

A-1. Ion current at 48 amu as a function of the residence time of CH_3O_2H in the reactor. For data taken at 553 K, the initial CH_3O_2H pressure was 0.8 torr; the pure CH_3O_2H was diluted to 52 torr total pressure with argon after 40 sec of reaction, producing the small break in the curve. At 513 K, the initial pressures were CH_3O_2H = 0.55 torr and Ar = 50 torr.

APPENDIX

As stated in the Experimental Section, the response of the mass spectrometer to CH_3O_2H was calibrated by injection of the pure compound into the reactor at 553 K. During the course of this calibration procedure, the intensity of the parent ion signal (48 amu) and the principal fragment (47 amu) decreased, indicating that the compound was being consumed. Figure A-1 presents CH_3O_2H ion-current vs time profiles obtained at two temperatures, which allow us to estimate the rate of decay of CH_3O_2H in our reactor. At 553 K, the rate of consumption was nearly exponential over approximately a factor of 10 in concentration. The first forty seconds of the plotted data were obtained with only CH_3O_2H in the reactor at an initial pressure of 0.8 torr. After this initial period, 52 torr of argon was introduced into the reactor causing a small change in the ion current. However, there was no significant change in the decay rate at the higher pressure, indicating that the rate is not very pressure dependent under these conditions.

The first order rate constant determined from these data is 8.5×10^{-3} sec^{-1} at 553 K. At 513 K the rate constant in the presence of 50 torr of argon is 2.7×10^{-3} sec^{-1}, which indicates that the apparent activation energy is approximately 16 kcal/mole. This value is much smaller than the 44 kcal/mole endothermicity of the homogeneous reaction 29 [114] and smaller than the 38-40 kcal/mole activation energies measured in the pyrolysis of larger aldyl hydroperoxides [115]. It is probable that wall catalysis or free radical chain reactions are occurring in our measurements, which increase the rate of CH_3O_2H consumption; the wall catalysis would significantly decrease the activation energy below that of the homogeneous reaction. For these reasons, the rate constants presented above are upper limits to the homogeneous, unimolecular rate of reaction 29. The upper limit at 553 K (8.5 x 10^{-3} sec^{-1}) is a factor of 6 smaller than an estimate of the homogeneous rate constant by Benson [29]. The expression presented in Table II was obtained from our upper limit at 553 K using Benson's reasonable estimate of 43 kcal/mole for the activation energy of the homogeneous reaction.

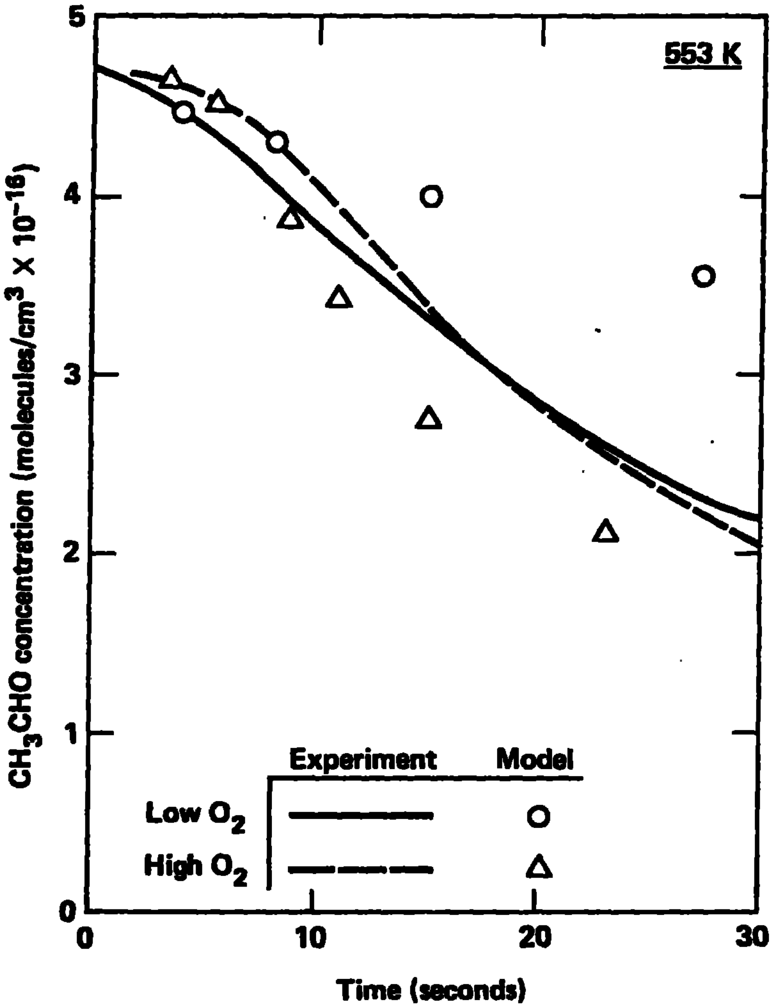
553 K
CH_3CHO concentration (molecules/cm^3 × 10^{-16})
Time (seconds)
0
1
2
3
4
5
0
10
20
30
Experiment
Model
Low O_2
○
High O_2
△

Fig. 1

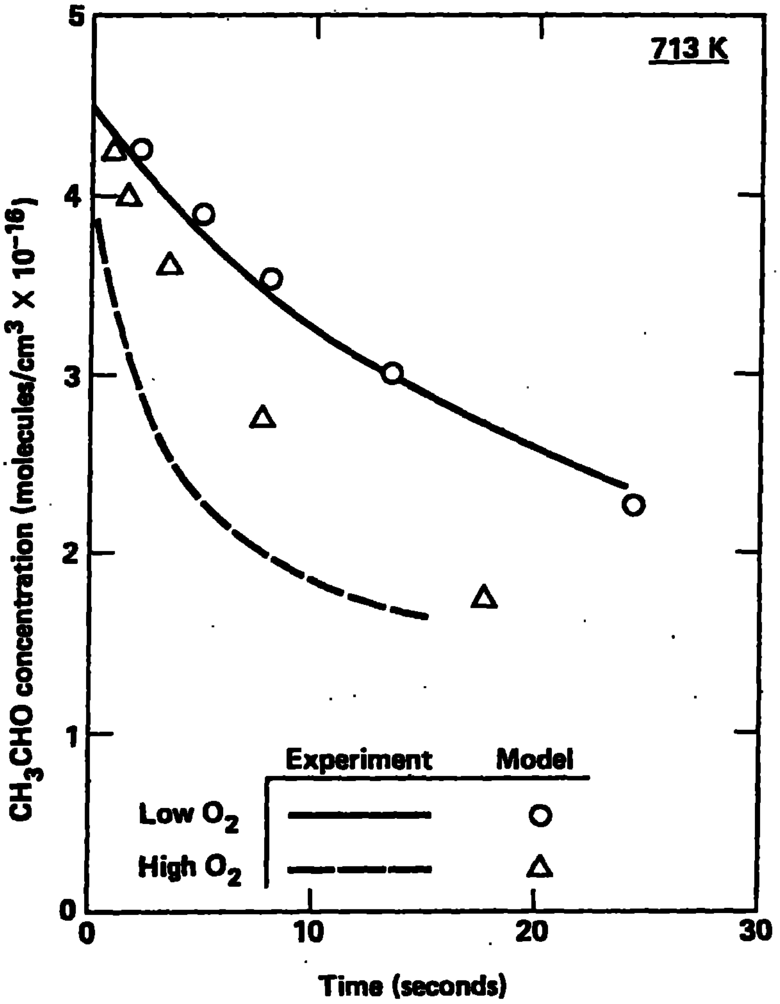
713 K
CH3CHO concentration (molecules/cm3 × 10−16)
Time (seconds)
0
1
2
3
4
5
0
10
20
30
Experiment
Model
Low O2
High O2

Fig. 2

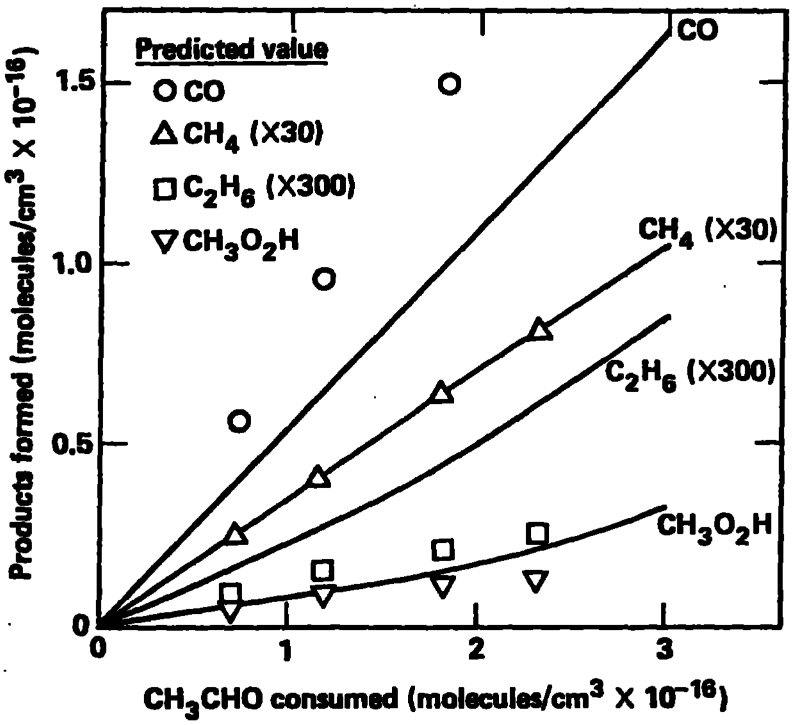
Predicted value
○ CO
△ CH4 (X30)
□ C2H6 (X300)
▽ CH3O2H
CO
CH4 (X30)
C2H6 (X300)
CH3O2H
Products formed (molecules/cm3 X 10-16)
0
0.5
1.0
1.5
0
1
2
3
CH3CHO consumed (molecules/cm3 X 10-16)

Fig. 3a

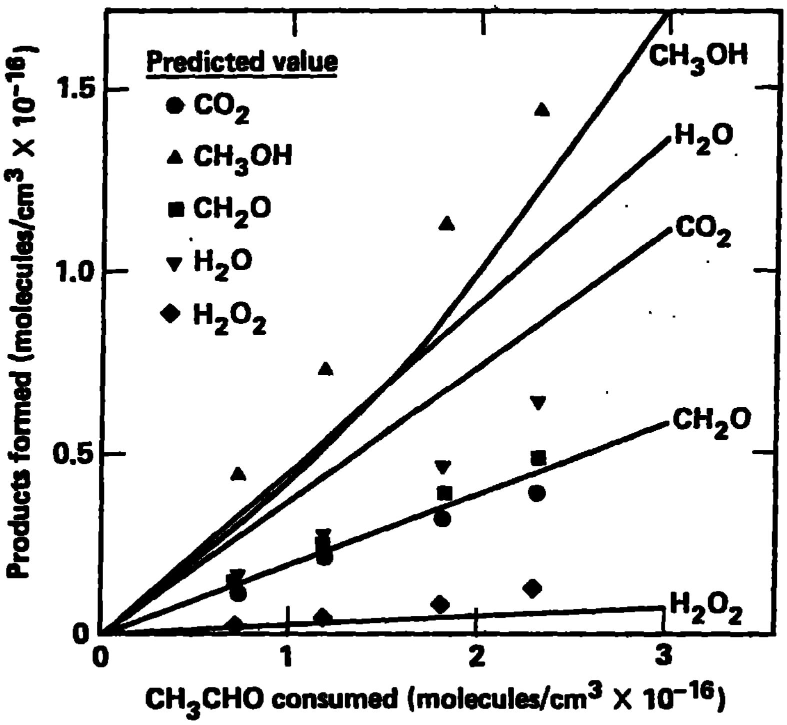
Predicted value
● CO_2
▲ CH_3OH
■ CH_2O
▼ H_2O
◆ H_2O_2
CH_3OH
H_2O
CO_2
CH_2O
H_2O_2
Products formed (molecules/cm^3 × 10^{-16})
0
0.5
1.0
1.5
0
1
2
3
CH_3CHO consumed (molecules/cm^3 × 10^{-16})

Fig. 3b

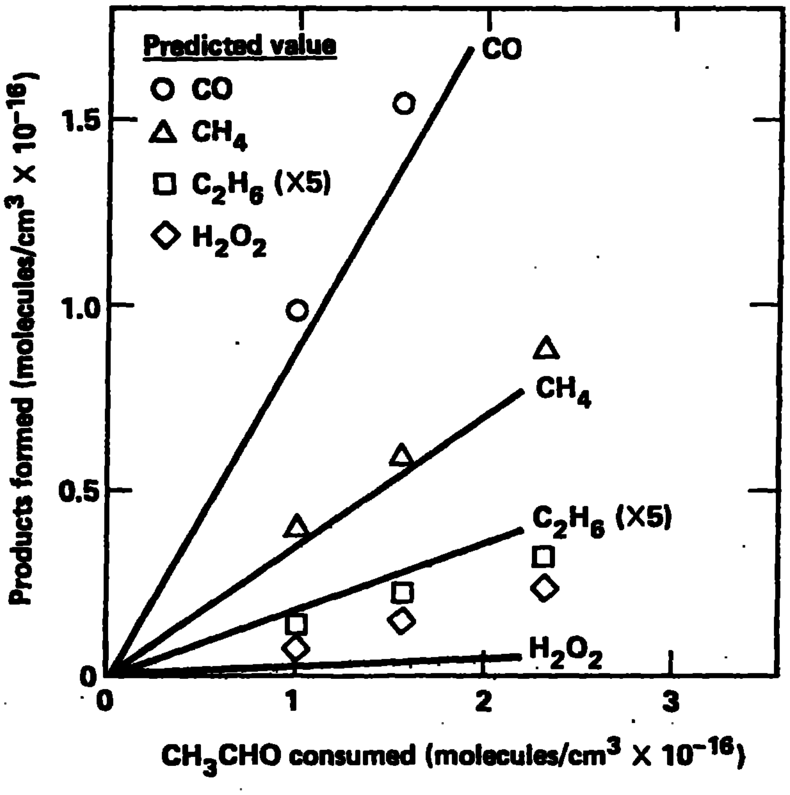
Predicted value
○ CO
△ CH_4
□ C_2H_6 (X5)
◇ H_2O_2
CO
CH_4
C_2H_6 (X5)
H_2O_2
Products formed (molecules/cm^3 X 10^{-16})
0
0.5
1.0
1.5
0
1
2
3
CH_3CHO consumed (molecules/cm^3 X 10^{-16})

Fig. 4a

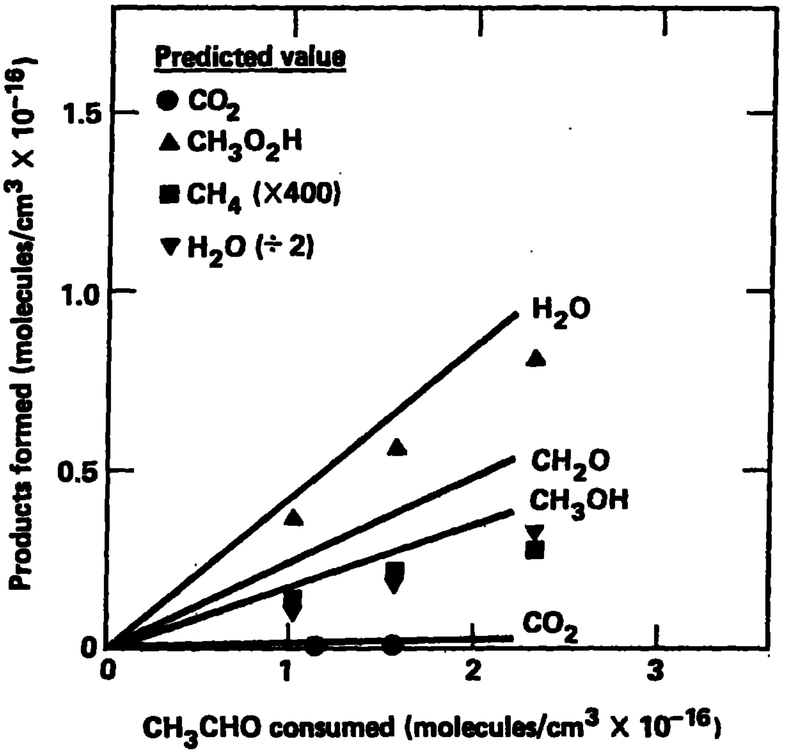
Predicted value
● CO_2
▲ CH_3O_2H
■ CH_4 (X400)
▼ H_2O (÷ 2)
H_2O
CH_2O
CH_3OH
CO_2
Products formed (molecules/cm^3 X 10^{-16})
0
0.5
1.0
1.5
0
1
2
3
CH_3CHO consumed (molecules/cm^3 X 10^{-16})

Fig. 4b

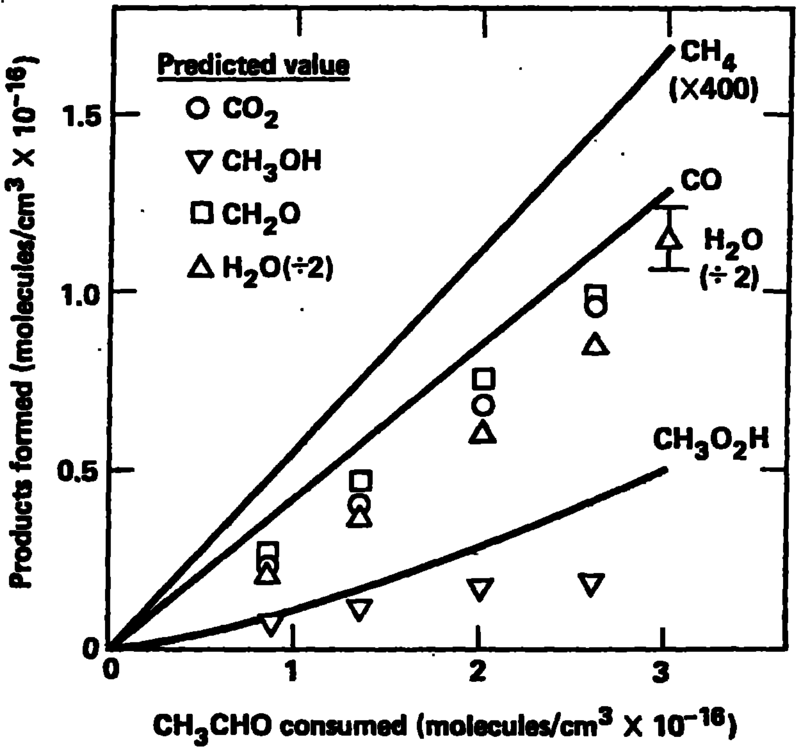
Predicted value
○ CO_2
▽ CH_3OH
□ CH_2O
△ $H_2O(\div 2)$
CH_4 (X400)
CO
H_2O ($\div$ 2)
CH_3O_2H
Products formed (molecules/cm^3 X 10^{-16})
CH$_3$CHO consumed (molecules/cm^3 X 10^{-16})
0
0.5
1.0
1.5
0
1
2
3

Fig. 5a

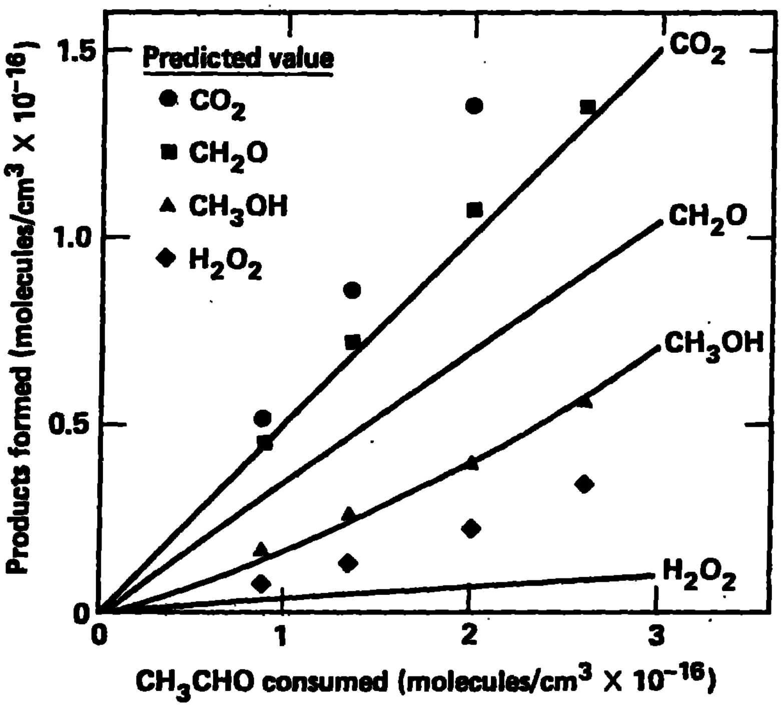
Predicted value
● CO_2
■ CH_2O
▲ CH_3OH
◆ H_2O_2
CO_2
CH_2O
CH_3OH
H_2O_2
Products formed (molecules/cm^3 X 10^{-16})
0
0.5
1.0
1.5
0
1
2
3
CH_3CHO consumed (molecules/cm^3 X 10^{-16})

Fig. 5b

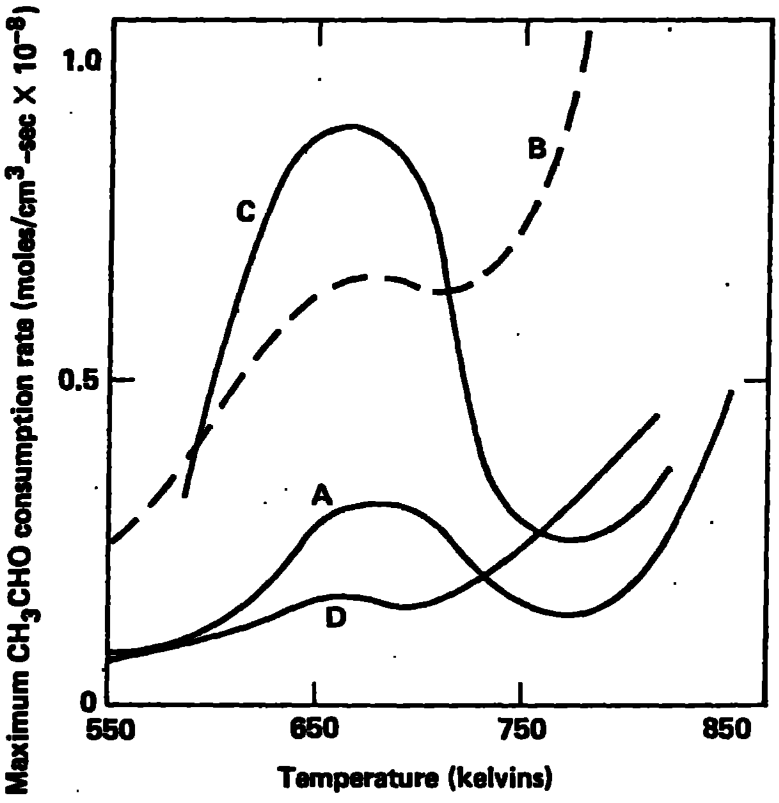
Maximum CH_3CHO consumption rate (moles/cm^3-sec × 10^{-8})
1.0
0.5
0
550
650
750
850
Temperature (kelvins)
A
B
C
D

Fig. 6

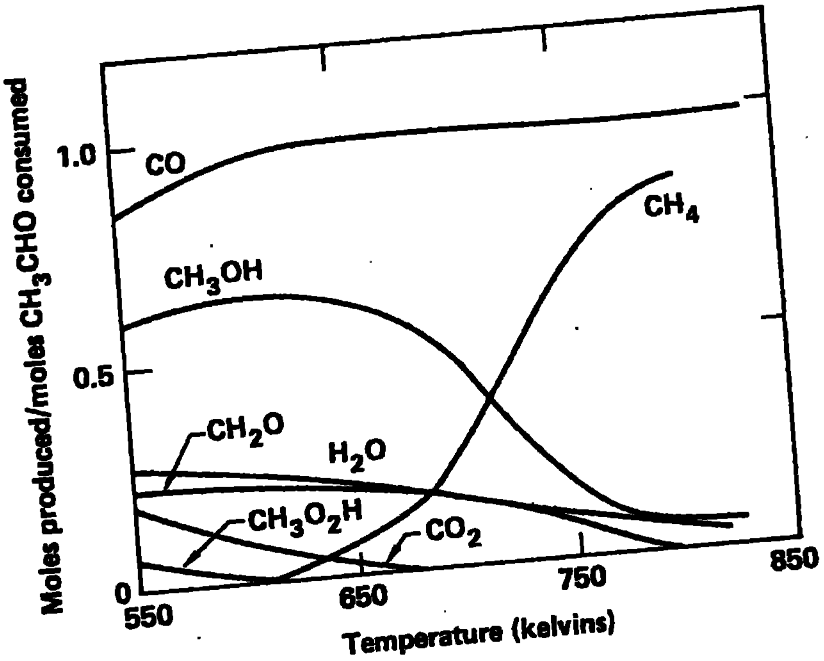
Moles produced/moles CH_3CHO consumed
1.0
0.5
0
550
650
750
850
Temperature (kelvins)
CO
CH_4
CH_3OH
CH_2O
H_2O
CH_3O_2H
CO_2

Fig. 7

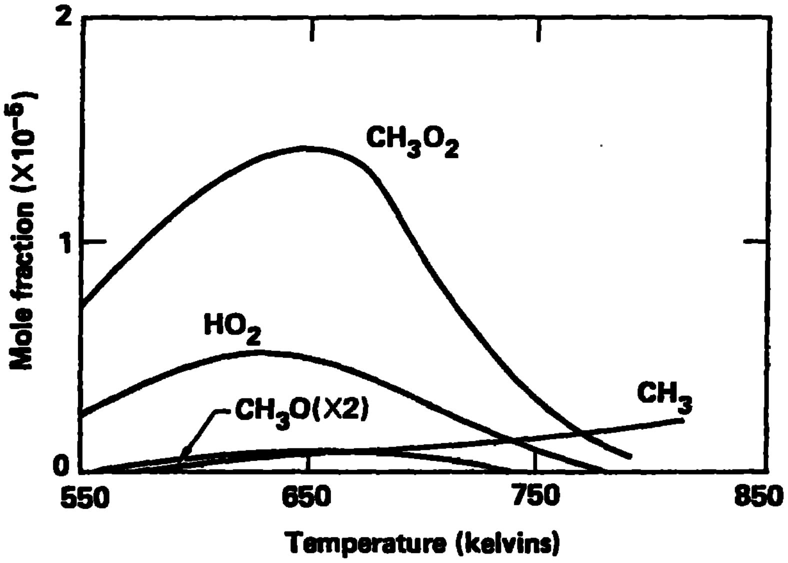
2
1
0
550
650
750
850
Temperature (kelvins)
Mole fraction (X10⁻⁶)
CH₃O₂
HO₂
CH₃O(X2)
CH₃

Fig. 8

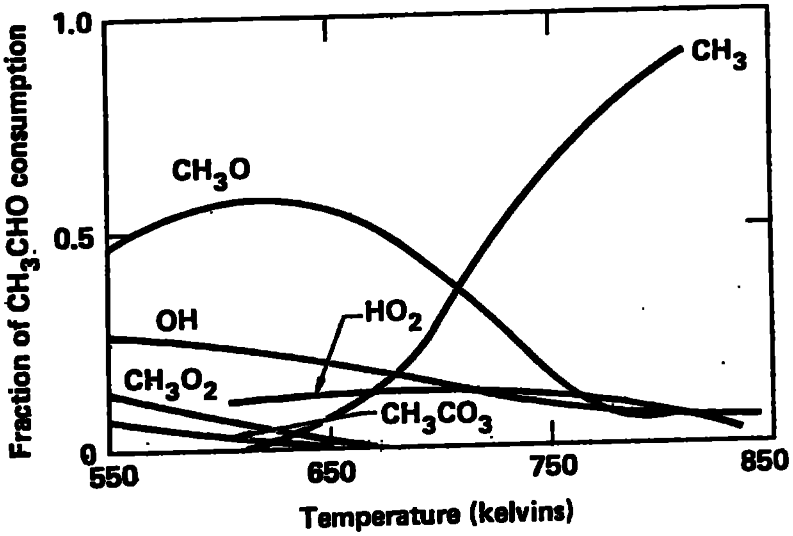
Fraction of CH3CHO consumption
1.0
0.5
0
550
650
750
850
Temperature (kelvins)
CH3
CH3O
OH
HO2
CH3O2
CH3CO3

Fig. 9

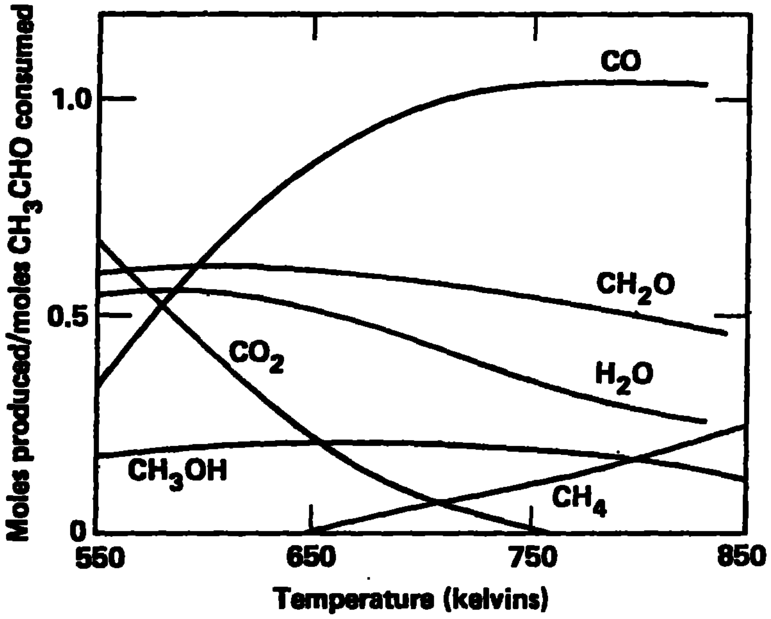
Moles produced/moles CH_3CHO consumed
1.0
0.5
0
550
650
750
850
Temperature (kelvins)
CO
CH_2O
H_2O
CO_2
CH_3OH
CH_4

Fig. 10

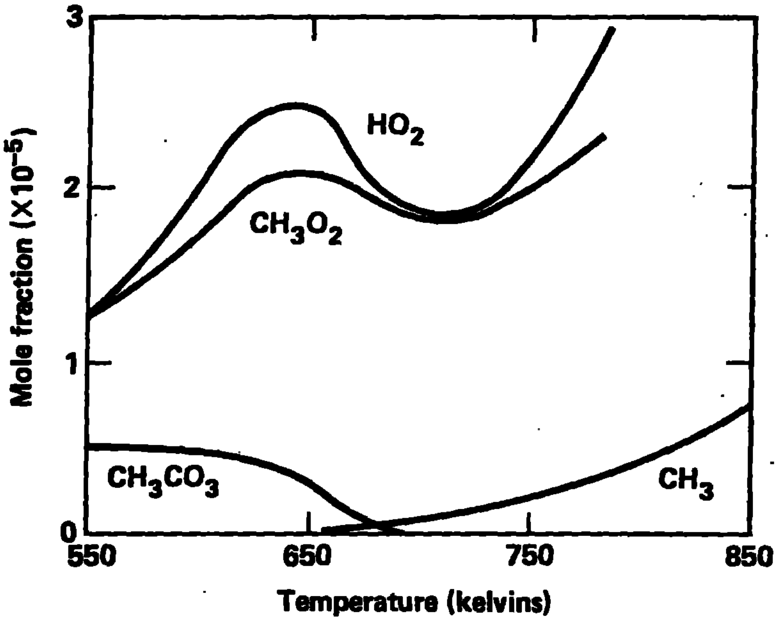
3
2
1
0
550
650
750
850
Mole fraction (X10^{-5})
Temperature (kelvins)
HO_2
CH_3O_2
CH_3CO_3
CH_3

Fig. 11

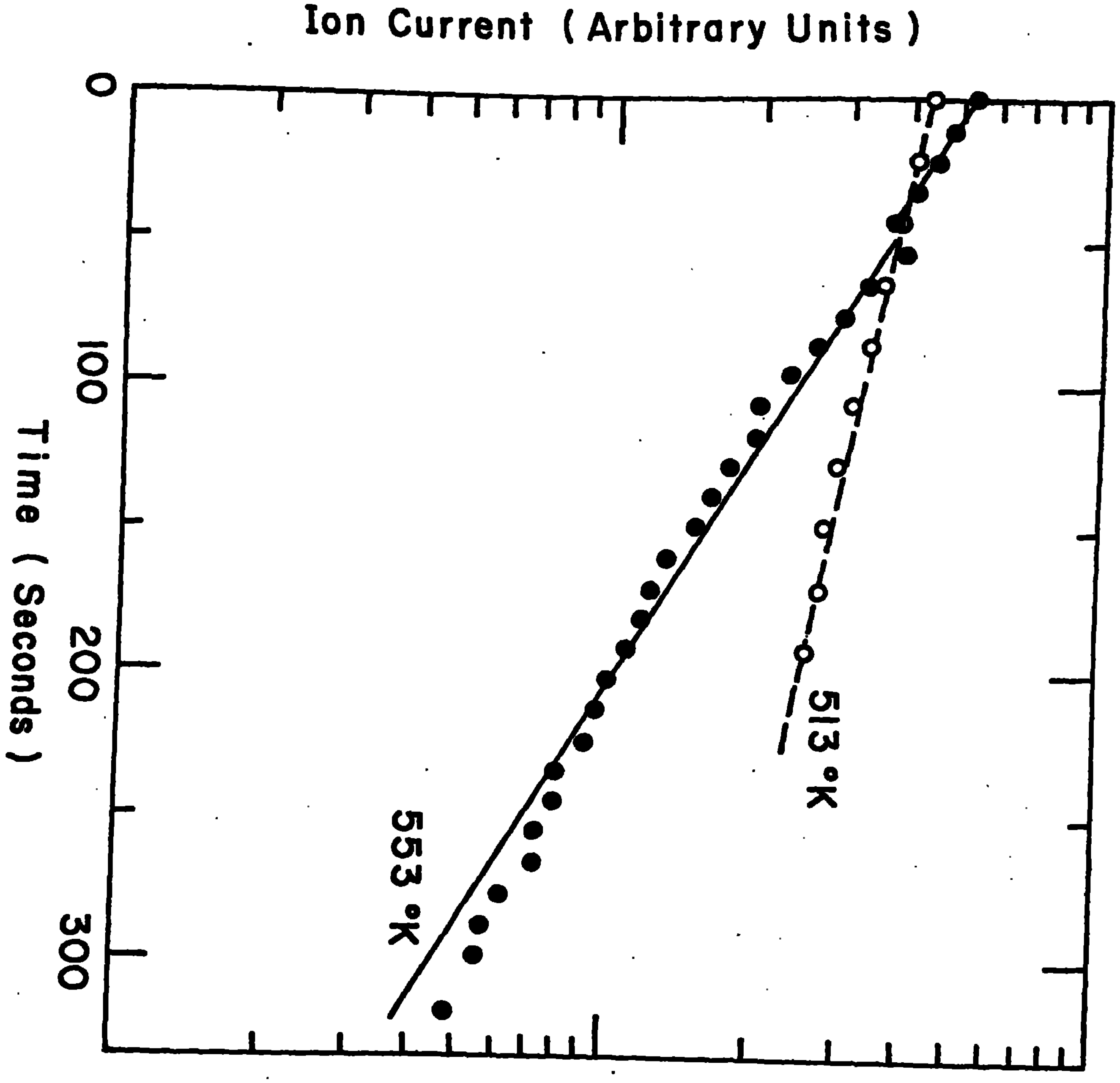
Ion Current (Arbitrary Units)
Time (Seconds)
0
100
200
300
513 °K
553 °K

Fig. A-1